Received: 18 December 2019 | Revised: 13 July 2020 | Accepted: 21 July 2020

DOI: 10.1002/cjce.23959

THE CANADIAN JOURNAL OF CHEMICAL ENGINEERING

Canadian Society for Chemical Engineering | For Our Future
Société canadienne de génie chimique | Pour notre avenir

MINI-REVIEW

Review on the structure of random packed-beds

Jennie von Seckendorff[1,2,3] | **Olaf Hinrichsen**[1,2]

[1]Department of Chemistry, Technical University of Munich, Garching, Germany

[2]Catalysis Research Center, Technical University of Munich, Garching, Germany

[3]BU Catalysts, Clariant Produkte (Deutschland) GmbH, Bruckmühl, Germany

Correspondence
Jennie von Seckendorff, Clariant Produkte (Deutschland) GmbH, Waldheimer Straße 13, 83052 Bruckmühl, Germany.
Email: jennieseckendorff@gmail.com

Abstract

Independent from their intended purpose, the understanding of structural characteristics of random packings of particles having defined shapes is important to understand and optimize fluid dynamic behaviour, heat, and mass transfer. The packing structure can be described by the coordination number, local porosity profiles, the average porosity, and pore characteristics, which are influenced by the wall and thickness effect; the material, shape, and size distribution of the packing particles; the packing and compaction mode; and the shape and material of the packing's containing walls. Therefore, existing knowledge on the structure of randomly packed mono-sized particles is reviewed to provide an updated selection of relevant parameters and their derived correlations obtained by experimental, numerical, and analytical means.

KEYWORDS

packed-bed reactor, porosity, random particle packings, review, structure

1 | INTRODUCTION

Random packings of particles having defined shapes are deployed in all kinds of industrial applications and come in all orders of magnitude. The most prominent examples comprise micro-sized particle beds as commonly used in chromatography packed columns,[1–3] packed-bed reactors filled with catalytic shaped bodies having millimetre size,[4,5] packed columns used in separation processes such as distillation incorporating particles in the lower centimetre range,[6,7] and the pebble-bed reactor, which is a gas-cooled nuclear reactor, moderated by a packing of graphite spheres.[8–10] In addition to those, numerous less-known applications of packed-beds exist, ranging from powder-bed 3D printers,[11] solar-energy storage systems,[12] earth science,[13] civil engineering,[14,15] and pharmaceutical processing,[16] to the pyrolysis of pelletized wood fuels,[17] to name but a few.

Irrespective of its intended purpose, the extent of a packed-bed is limited by a confining wall of commonly cylindrical shape, though flat plates and other container geometries are possible. Despite its generally random nature, close to this confinement the particles' placement is naturally forced to align with the wall's geometry. This imposed order reaches a couple of particle diameters into the packing and is usually named the wall effect. Its influence on the overall packed-bed characteristics decreases with increasing tube-to-particle diameter ratio $\lambda = \frac{D}{d_p}$. While most applications operate in an only sparsely affected λ-range, this effect becomes dominant, for instance, in catalytic multitubular reactors, typically performing at λ = 4-7[18] or a single-pellet-string reactor with a $\lambda < 2$.[19] Moreover, some packed-bed utilizations, especially chromatography columns, have very delicate requirements regarding bed homogeneity and its derived characteristics.

Abbreviations: DEM, discrete element method; Erfc, error function; J_0, Bessel function of first kind and zero order; MRJ, maximally random jammed; RCP, random close packing; RLP, random loose packing.

In general, random packed-beds are typically investigated in regard to the void distribution,[20,21] single- and multi-phase flow aspects,[22] the extent of pressure loss along the bed height,[23] axial and radial dispersion qualities[24] in common with inter- and intraparticle heat,[25] and mass transfer properties. In this contribution, parameters that describe and influence the structural characteristics are reviewed, clustered, and compared. Parameters describing the packing structure comprise the coordination number $\bar{N}_c$, the radial porosity distribution $\varepsilon(r)$, the axial porosity distribution $\varepsilon(z)$, the average bed porosity $\bar{\varepsilon}$, and the pore size characteristics. These parameters are influenced by the wall effect, the thickness effect, the packing and compaction mode, the particle material, shape and size distribution, and the container's shape and material. Results can be obtained by partially elaborate experiments; however, the sheer number of recently published numerical approaches,[26] including the generation of random packed-beds using, for instance, the discrete element method (DEM) with subsequent flow, heat, and/or mass transfer simulation by known tools such as COMSOL Multiphysics®, Ansys Fluent®, STAR-CCM+®, or OpenFOAM®, speaks for itself. Although the developed numerical procedures require delicate validation, the gain in knowledge from employing the detailed resolution and visualization options is impressive.

The focus of this contribution is to review the different published methodologies and results to characterize the structure of random packed-beds using both experimental and numerical approaches.

2 | EXPERIMENTAL INVESTIGATION OF PACKED-BED STRUCTURES

Random packings of particles having a distinct shape are characterized by the size, distribution, and the mean void fraction of the voids between the solids (porosity ε), the coordination number $\bar{N}_c$ describing the average number of contact points between adjacent particles, and their average contact angle $\bar{\phi}_c$. Besides the tube-to-particle diameter ratio λ, these parameters may be influenced by the particle's material, shape and size distribution, the container's material and shape, and the applied deposition and compaction methods.[27,28]

2.1 | Regular arrangements of spatially extended mono-sized ideal spheres

Regular arrangements of spheres are characterized by a repeating pattern whose smallest repetition unit, the unit cell, represents the whole packing. It is the simplest case of a packed-bed and its structural characteristics can be derived by mathematical considerations.[29,30] Table 1 summarizes typical arrangements and their quantities. For more details, see the relevant reviews on this topic.[13,21,31,32] Although these packed-beds are usually not utilized directly, they define the maximum porosity range a sphere packing can adapt to in the absence of a confining wall. Here, Taylor et al[14] defined the packing factor α_m as the ratio between the volumes of the unit cells of the actual packing and the cubic packing of which the packing properties are compared. Moreover, regular arrangements can be used as a starting point to derive models for more realistic sphere packings,[33] liquids,[34] or other porous systems.[14,15]

2.2 | Random packings of smooth mono-sized ideal spheres in cylindrical confining walls

Random packings of smooth, mono-sized, ideally spherical particles in cylindrical confining walls are frequently taken as the standard or reference packing arrangement. It is by far the most evaluated and researched packed-bed configuration, though in many cases not adequately representing the reality in industry.

2.2.1 | Coordination number and angle

The number of contact points between one particle and its neighbours in combination with the angular distribution of these along the surface of the particles is of special interest for heat transfer investigations[35] and the general modelling of transport phenomena.[36] While regular packings have one distinct coordination number for each arrangement, varying from 6-12 (Table 1), random packings are characterized by having a distribution of coordination numbers.

TABLE 1 Characteristics of regular sphere packings[14,29–31]

Arrangement	Coordination number N_c (–)	Mean bed porosity $\bar{\varepsilon}$ (–)	Packing factor α_m (–)
Cubic	6	0.476	1
Orthorhombic	8	0.395	$\sqrt{3}/2$
Body-centred cubic	8	0.320	
Tetragonal-sphenoidal	10	0.302	0.75
Rhombohedral	12	0.260	$\sqrt{2}/2$

Experimental

The traditional experimental evaluation of the coordination number is obtained by filling the voids within a packed-bed of spheres with a marker liquid. After drainage, the marker liquid will be retained at the true contact points by capillary forces.[37] Furthermore, near contact points are marked as well, as capillary forces allow bridging of narrow gaps.[38] True and near contact points can be distinguished, as a circle of marker substance with a non-marked centre indicates true contact points, whereas near contact points are marked by a filled circle.[38] The number and the distribution of true and near contacts can be obtained by counting the marker dots on each sphere. The mean coordination numbers and their cumulative frequency distribution as obtained by experiments are displayed in Figures 1 and 2.

Some of the first researchers to address the experimental evaluation of the coordination number was Smith et al.[37] They used a packing of lead shot and acetic acid, forming white lead acetate as marker liquid. However, it was noted that the data was erroneous[21] and it was eventually re-evaluated by Wadsworth.[39]

A similar approach was selected by Bernal and Mason,[38] except for the fact that they used ball bearings with black paint as a marker. They were the first to distinguish between true and near contacts and investigated two packed-bed densities. The same procedure was selected by Oda,[42] investigating mono-sized sphere packings as well as binary and quaternary mixtures. While Arakawa and Nishino[40] used red ink to mark contact points between spheres, the utilization of shellac in methylated spirit was preferred by Pinson et al[41] and Zou et al.[47]

A completely different approach was selected by Goodling and Khader.[36] Here, a packed-bed of spheres was solidified with epoxy resin, layers were cut, and photographs were taken. It was ensured that each sphere was cut at least twice so that the centre of each sphere could be determined. The contact points of each sphere were then obtained by mathematical considerations.

Modern imaging techniques allow the highly resolved determination of packed-bed structures. Aste et al[44,45] used X-ray computed tomography for the evaluation of the contacts between mono-sized spheres. Here too, uncertainty remained as to the distinction between true and near contacts due to voxel resolution. Similar studies were performed by Georgalli and Reuter,[48] Reimann et al,[49–51] and Auwerda et al.[46]

The radial distribution function

For further investigations of the contact behaviour, Scott[52] determined the sphere centres in a packed-bed by filling the voids with molten wax, and after solidification removed each sphere separately from the matrix while noting each sphere's position. From this, he computed a radial density distribution using the distance normalized by the sphere diameter of the centres of the spheres from the wall of the random packed-bed. This distribution was averaged for 25 randomly selected spheres. Mason and Clark[53,54] added a direct sphere distance measuring technique in order to refine the near contacts portion.[38] The obtained plot is known as the *radial distribution function* and is used to model fluids (spheres represent atoms or molecules) or colloids (see Scott and Mader,[55] Finney,[56] Urquidi et al,[57] Dohn

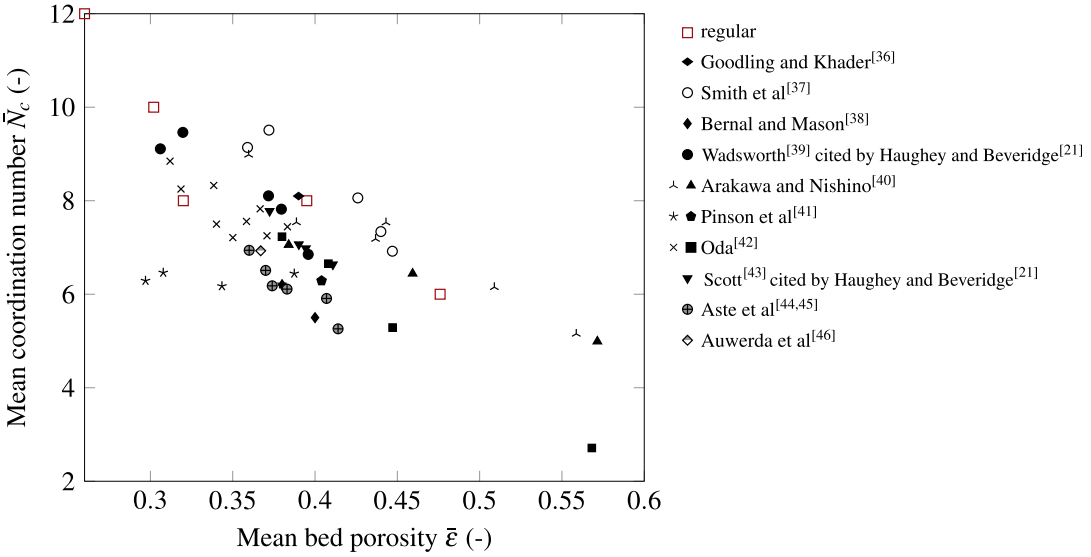

FIGURE 1 Experimental results obtained from the literature for the mean coordination number $\bar{N}_c$ as a function of porosity $\bar{\varepsilon}$. Full symbols represent data of homogeneous spheres, crosses those of size mixtures[21,39–46]

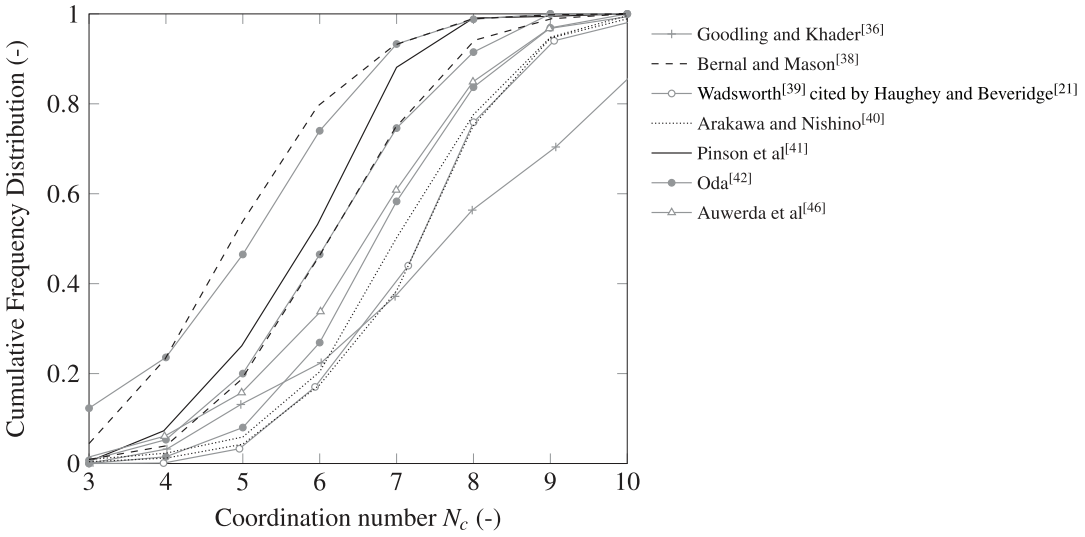

FIGURE 2 Experimental results obtained from the literature for the cumulative frequency distribution of the mean coordination number $\bar{N}_c$[21,36,38–42,46]

et al,[58] and Soper.[59]) It is to be noted that any investigation of radial distribution functions requires the absence of confinement influence.

Extrapolation and analytical considerations

When it comes to deriving mean contact number-porosity correlations it has to be considered that stable and realistic sphere packings only come in a small porosity range. It is generally accepted that the simple cubic arrangement constitutes the lower limit of a stable sphere packing. The range of realistic packings is even smaller. In order to overcome this barrier, Meissner et al[60] tried to extrapolate available coordination number data by investigating sphere arrangements looser than the regular cubic packing. Similar approaches were performed by Melmore[61] and Heesch and Laves.[62] Further analytical investigations regarding extra loose sphere packings were performed in the context of sedimentation processes.[63,64] Bennett[65] investigated packings artificially packed according to local and global criteria.

A completely different approach to overcome the problem that stable sphere packings only come in a very small porosity range is proposed by evaluating micro- and nanosized particles, as the porosity increases with decreasing particle size.[66–69] However, in this size range, the contact behaviour can only be determined numerically.[66,70]

In contrast to this, pure analytical approaches were described by Liu and Davies,[71] who derived sphere contact information from the radial distribution function. Beck and Volpert[72] used the gapped gapless packing model[73–76] in combination with a fixed fraction annular and a self-same contact distribution to derive the contact behaviour of homogeneous spheres and binary mixtures. A similar approach was used by Richard et al,[77] incorporating radical and Voronoï tessellation as well as the navigation map. Other analytical-parametric models were developed by Yu and Standish[78] and Iwata and Homma.[79]

Furthermore, investigations of the contact behaviour of numerically generated packed-beds were conducted.[70,80–90] Among these, Clarke and Jónsson[86] could confirm the results of Bernal and Mason.[38] Most others focussed on multi-component packings. An et al[90] tried to determine whether the packing of uniform spheres under gravity is quasi-universal. Therefore, extensive numerical screening was done, trying to extrapolate the known results by comparing micro- and normal-sized particles, vibrated and non-vibrated beds, filling beds in liquid, and air surroundings. Packing porosities between 0.8-0.26 are obtained, relating to a clear trend in regard to the coordination number.

Results collected from the literature

A comprehensive selection of derived correlations obtained by the above-described experiments, analytical models, and extrapolation approaches is summarized in Figure 3 and Table 2.

The mean coordination number of sphere packings as obtained by experiments ranges from 6-8. From regular packings it is obvious that a packed-bed may have different coordination numbers for the very same porosity (refer to Table 1). Incorporating analytical and numerical data, a mean coordination number of around 6 is generally accepted for a typical packed-bed of mono-sized spheres.[41,44,45,47,56,70,85,87,88,101] For a random close packing, a value of up to 7 is determined.[44,45,49] Deviations between experiments are often explained by the poor discrimination of true and near contacts.

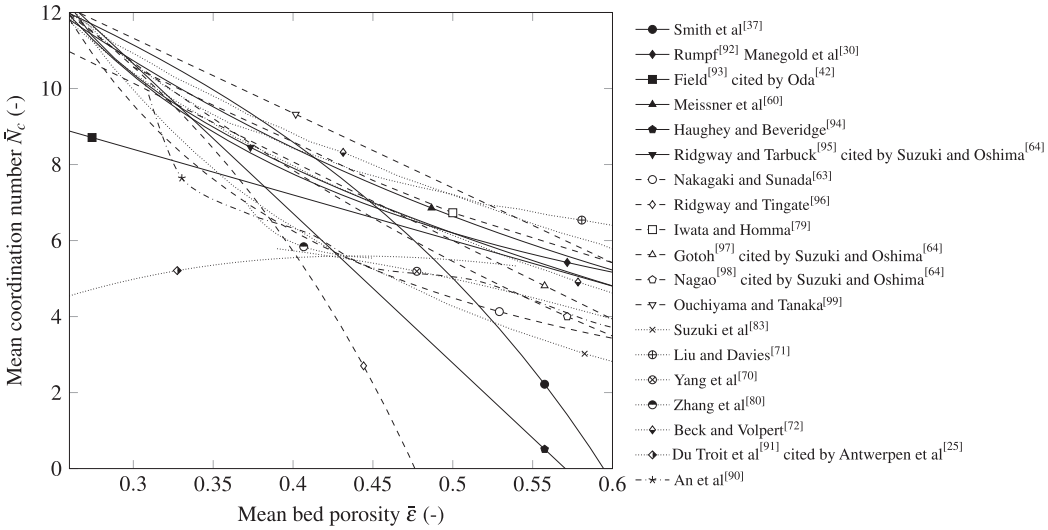

FIGURE 3 Comparison plot of known correlations regarding the relation of mean coordination number $\bar{N}_c$ and mean packed-bed porosity $\bar{\varepsilon}$ for random packings and abstract arrangements of mono-sized spheres[25,30,37,42,60,63,64,70–72,79,80,83,90–99]

TABLE 2 Overview of known correlations relating the mean contact number $\bar{N}_c$ to the packing porosity $\bar{\varepsilon}$ of smooth mono-sized sphere packings

Source	Formula	Scope
Smith et al[37]	$\bar{N}_c = \frac{15.75-26.49\cdot\bar{\varepsilon}}{1-\bar{\varepsilon}}$	$0.259 < \bar{\varepsilon} \le 0.476$
Rumpf[92] and Manegold et al[30]	$\bar{N}_c = \frac{3.1}{\bar{\varepsilon}}$	$0.259 < \bar{\varepsilon} \le 1$
Field[93] cited by Oda[42]	$\bar{N}_c = 12\cdot(1-\bar{\varepsilon})$	n.a.
Meissner et al[60]	$\bar{N}_c = 2\cdot\exp(2.4\cdot(1-\bar{\varepsilon}))$	$0.259 < \bar{\varepsilon} \le 1$
Haughey and Beveridge[94]	$\bar{N}_c = 22.47-39.39\cdot\bar{\varepsilon}$	$0.259 < \lambda \le 0.5$
Ridgway and Tarbuck[95] cited by Suzuki and Oshima[64]	$\bar{N}_c = 13.84-116\cdot(0.01724\cdot\bar{\varepsilon}-0.00428)^{1/2}$	$0 < \bar{\varepsilon} \le 0.82$
Nakagaki and Sunada[63]	$\bar{N}_c = 1.61\cdot\bar{\varepsilon}^{-1.48}$	$0 < \bar{\varepsilon} \le 0.82$
Ridgway and Tingate[96]	$\bar{N}_c = 24-\frac{2}{3}\cdot\left(\frac{\pi}{1-\bar{\varepsilon}}\right)^2$	$0.26 < \bar{\varepsilon} \le 0.47$
Gotoh[97] cited by Suzuki and Oshima[64]	$\bar{N}_c = 20.7\cdot(1-\bar{\varepsilon})-4.35$	$0.3 < \bar{\varepsilon} \le 0.53$
	$\bar{N}_c = 36\cdot\frac{1-\bar{\varepsilon}}{\pi}$	$\bar{\varepsilon} > 0.53$
Nagao[98] cited by Suzuki and Oshima[64]	$\bar{N}_c = 21.80\cdot(1-\bar{\varepsilon})^2$	n.a.
Ouchiyama and Tanaka[99]	$\bar{N}_c = \frac{32}{13}\cdot(7-8\cdot\bar{\varepsilon})$	n.a.
Suzuki et al[83] cited by Suzuki and Oshima[64]	$\bar{N}_c = 2.812\cdot\frac{(1-\bar{\varepsilon})^{-1/3}}{\left(b/d_p\right)^2\cdot\left[1+\left(b/d_p\right)^2\right]}$	$0.24 < \bar{\varepsilon} \le 0.54$
	with $(1-\bar{\varepsilon})^{-1/3} = \frac{1+\left(b/d_p\right)^2}{1+\left(b/d_p\right)\cdot\exp\left(d_p/b\right)^2\cdot Erfc\left(d_p/b\right)}$	
Suzuki et al[100] cited by Georgalli and Reuter[48]	with $\frac{b}{d_p} = 0.07318+2.193\cdot\bar{\varepsilon}-3.357\cdot\bar{\varepsilon}^2+3.294\cdot\bar{\varepsilon}^3$	
Liu and Davies[71]	$\bar{N}_c = (1-\bar{\varepsilon})\cdot\left(\frac{b}{r}\right)^3-1+$	$0.22 < \bar{\varepsilon} \le 0.66$
	$+\frac{24\cdot(1-\bar{\varepsilon})\cdot a\cdot(a^2-c^2)}{r^3\cdot(a^2+c^2)^3}+\frac{6\cdot(1-\bar{\varepsilon})\cdot(3a^2-c^2)}{r^2\cdot(a^2+c^2)^2}\cdot\frac{b}{r}+\frac{6\cdot(1-\bar{\varepsilon})\cdot a}{r\cdot(a^2+c^2)}\cdot\left(\frac{b}{r}\right)^2$	
	with $b = 2\cdot r+\frac{1}{c}\left(\frac{\pi}{2}+\arctan\frac{c}{a}\right)$, $a = \frac{2\cdot\pi}{r}\left[4\cdot\pi\cdot\left(\frac{\bar{\varepsilon}}{1-\bar{\varepsilon}}\right)^2\right]$ and $c = 2\cdot\pi\cdot\frac{1-\bar{\varepsilon}}{r}$	
Yang et al[70]	$\bar{N}_c = 2.02\cdot\frac{1+87.38\cdot(1-\bar{\varepsilon})^4}{1+25.81\cdot(1-\bar{\varepsilon})^4}$	$0.39 < \bar{\varepsilon} \le 1$
Zhang et al[80]	$\bar{N}_c = \frac{1}{0.183-659.248\cdot(1-\bar{\varepsilon})^{20.961}}$	$0.37 < \bar{\varepsilon} \le 0.45$
Du Toit et al[91] cited by Antwerpen et al[25]	$\bar{N}_c = 25.952\cdot\bar{\varepsilon}^3-62.362\cdot\bar{\varepsilon}^2$ $+39.724\cdot\bar{\varepsilon}-2.02$	$0.24 < \bar{\varepsilon} \le 0.54$

While most researchers exclude the particles close to the confining walls, the wall effect on the mean coordination number was explicitly investigated by Pinson et al,[41] Goodling and Khader,[36] Auwerda et al,[46] and Reimann et al.[49] A decrease in the coordination number is observed only for the outermost and potentially the second ring of spheres adjacent to the wall, whereas Du Toit et al[25,91] observed a significant difference in mean coordination number between bulk and near-wall region. Furthermore, Reimann et al[49] investigated the influence of the flat container bottom, finding a constant coordination number of 9 for the very bottom layer of spheres, while a coordination number of just below 12 could be obtained for the following three sphere layers in quasi-close packing conditions.

Contact angle

The angular distribution was experimentally determined by Scott and Mader,[55] finding certain angular structures at about 60°, 120°, and 180° by using an averaged polar plot of the surface of the spheres. Reimann et al[49,50] divided the contact angle into the poloidal angle ϕ_c, describing orientation along the container axis and the azimuthal angle ψ, describing the orientation in the radial direction. In the bulk region, the angle distribution is quite homogeneous, but developing a certain structure at 30° and 150° in the poloidal orientation and 0° and 180° in the azimuthal orientation close to the confining sidewall and bottom. Du Toit et al[25,91] found a mean bulk contact angle in the poloidal direction of 31.97° which was detected to relate to the coordination number according to Equation (1)[25]:

$$\bar{\phi}_c = -6.1248 \cdot \bar{N}_c^{\,2} + 73.419 \cdot \bar{N}_c - 186.68 \qquad (1)$$

2.2.2 | Radial porosity distribution

Regarding packings enclosed by a cylindrical wall, the structure of the random packings is typically characterized by plotting the circumferentially and axially averaged void space (porosity ε) against the radial position within the cylindrical tube starting at the tube wall and normalized to the particle diameter (d_p), $z_r = (R - r)/d_p$. The occurrence of local deviations from the theoretical bulk packing porosity in random packings is regarded as an indicator of the influence of the confining wall on the near-wall packing structure.

Experimental

Referring to Schneider and Rippin,[102,103] four kinds of general experimental procedures can be clustered to determine the local void fraction distribution within packed-beds:

1. The first is solidification and incremental removal. The experimental investigation of axially-averaged radial porosity profiles was historically conducted by filling the voids between the packing particles with molten wax or curable resins and the subsequent cutting or machining of the solidified matrix into thin radial or axial slices. Either the filler material is removed and the weight difference noted,[104–108] or photographs of the slices can be subjected to image analysis resulting in the filled void content of each slice.[103,109–115] Due to the small size of many packed-beds combined with the inaccuracy of cutting tools, these early investigations result in quite coarse and potentially erroneous curves. Moreover, loss of particles during the cutting procedure due to insufficient bonding strength between the particles and the filler material are commonly reported.[104,105,109] As an improvement, the resin can be mixed with metal powders[107] or hardening additives.[103,107]
2. Incremental filling is a completely different approach, comprising a centrifuged packed-bed to which small amounts of liquid, predominantly water, are added. The liquid forms an annular layer and the increment in layer thickness for a known amount of added water depends on the available void space, assuming a homogeneous void distribution for each radial section.[116–120] However, the precise determination of small variances in liquid level, especially considering the meniscus, makes this technique challenging. Lerou and Froment[119] improved this setup by accurately measuring the water level using a pressure transducer.
3. Individual particle measurement is the easiest way, if quite erroneous, involving the use a grid on a transparent container and counting the particles of which the centres are within a certain grid cell.[121] For more accurate results, the packed-beds can again be solidified with resin, and each and every sphere can be scratched out from the resin basis after noting its position.[52–54] Schuster and Vortmeyer[122] used a piston with sticky tape to remove the spheres of a packed-bed layer by layer, taking a photograph of each layer and subsequently allocating each sphere to a grid of position on the piston.
4. Projection of the bed is the last procedure. Initially, the solidified and cut packed-bed slices were scanned with an x-ray beam in order to improve data acquisition.[109] Later, x-ray tomography was used for non-destructive analysis of the whole packed-bed.[10,46,49,50,123–128] A stack of sliced packed-bed

images is obtained where subsequent image analysis has to be performed. Most frequently, the computer-based image analysis includes the binarization of the obtained grayscale images in order to specify solid and void area. From these, the void ratio at a certain radial position can be estimated directly or the centre position of each sphere can be determined, requiring the subsequent mathematical calculation of radial profiles. The specification of the black-white threshold is frequently identified as the major source of error. Additionally, Buchlin et al,[129] whose work was later adopted by Schneider and Rippin,[102] used the fluorescence of a slightly impure organic liquid having the same refractive index as transparent spheres to visualize the particle locations. Besides X-ray tomography, magnetic resonance imaging may be used as well to investigate local structures within packed-beds.[130–134] Again, a proper image analyzing procedure is required.[131]

Results collected from the literature

Regarding the obtained radial porosity data, some specific properties are generally accepted, including[20]:

- The porosity directly at the tube wall has a value of 1.
- The curve resembles a damped oscillatory function with distinct extrema until reaching 4-5 particle diameters into the tube.
- The first minimum is at $z_r = d_p/2$ and the first maximum is at $z_r = d_p$.

Further properties of the radial porosity distribution under discussion comprise the initial shape of two consecutive parabolas transitioning to a sinusoidal variation when moving further away from the tube wall, the non-constant period of oscillation within a specific bed, and the amplitude, which varies when different experimental results and the derived correlations are compared.[20]

Gathering the majority of experimental data ranging from $\lambda > 2$ to $>>10$ as presented in the literature into a single figure (Figure 4), reveals a surprising consensus even without preference in regard to packing mode and material specifications. Significant differences can be seen for packed-beds of low tube-to-particle diameter ratios where the values in the tube centre are significantly larger at $z_r \approx 1$ (data of Benenati and Brosilow,[105]) $z_r \approx 2$ (data of Lovreglio et al,[139] Mariani et al,[127] Mueller,[135] Wensrich[140]), $z_r \approx 3$ (data of Mueller[135]), and $z_r \approx 4$ (data of Lovreglio et al,[139] and Giese et al[136]).

In Figure 4, the experimental studies of Schwartz and Smith[141] and Shaffer[117] are not considered as absurd bulk porosity values for sphere packings of as low as 0.32 and 0.28 were obtained, respectively. Furthermore, the study of Pillai[121] and Korolev et al[123] could not be considered, as the data is incomplete. The study of Al-Falahi and Al-Dahhan[125] is not considered since obvious deviations from the generally accepted oscillatory behaviour is seen, as well as questionable porosity values close to the wall. The experimental study of Ismail et al[112,113] is not considered because the results for the radial porosity profile do not fit with all other results in the following points: the extrema positions are overall slightly shifted to higher numbers and the curve shape of especially the first maximum appears very smooth.

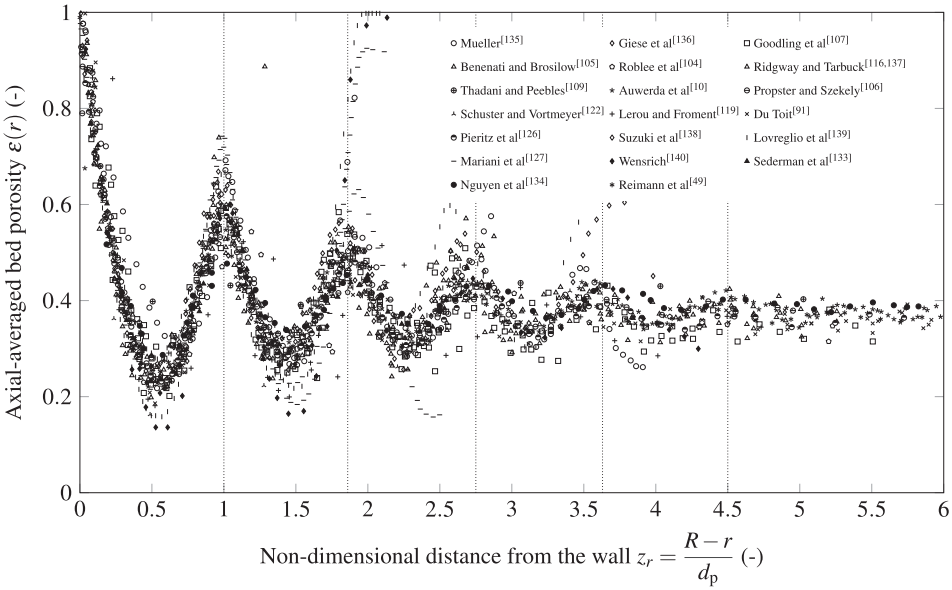

FIGURE 4 Gathered experimental literature data of radial porosity distributions $\epsilon(r)$ obtained by using various experimental methods and packing procedures and containing spheres of different materials enclosed by a cylindrical confining wall[10,49,91,104–107,109,116,119,122,126,127,133–140]

TABLE 3 Selection of known wall effect correlations for the radial void distribution $\epsilon(r)$ of spherical packed-beds in cylindrical confinements

Source	Formula	$\bar{\varepsilon}_{inf}$	Scope
De Klerk[20]	$\varepsilon(r) = 2.14 \cdot z_r^2 - 2.53 \cdot z_r + 1$	-	$z_r \leq 0.637$
	$\varepsilon(r) = \bar{\varepsilon}_{inf} + 0.29\exp(-0.6 \cdot z_r) \cdot [\cos(2.3 \cdot \pi \cdot (z_r - 0.16))] + 0.15\exp(-0.9 \cdot z_r)$	n.a.	$0.637 < z_r$
Johnson[142] cited by Roshani[103]	$\varepsilon(r) = \bar{\varepsilon}_{inf} + 0.62 \cdot \exp\left[-1.7 \cdot (z_r)^{0.434}\right] \cdot \left[\cos\left(6.67 \cdot (z_r)^{1.13}\right)\right]$	0.38	$z_r \leq 4$
	$\varepsilon(r) = \bar{\varepsilon}_{inf}$	0.38	$4 < z_r$
Moallemi[143] cited by Roshani[103]	$\varepsilon(r) = \bar{\varepsilon}_{inf} - 0.6 \cdot \left(1 - \exp\left[-1.7 \cdot (z_r)^{0.52}\right] \cdot \left[\cos\left(5.57 \cdot (z_r)^{1.25}\right)\right]\right)$	n.a.	n.a.
Chandrasekhara and Vortmeyer[144]	$\varepsilon(r) = \bar{\varepsilon}_{inf} \cdot (1 + b \cdot \exp(-c \cdot x))$ with $b = 1$ $c = 3$	n. a.	n. a.
Martin[145]	$\varepsilon(r) = \varepsilon_{min} + (1 - \varepsilon_{min}) \cdot (2 \cdot z_r - 1)^2$	-	$z_r \leq 0.5$
	$\varepsilon(r) = \bar{\varepsilon}_{inf} + (\varepsilon_{min} - \bar{\varepsilon}_{inf}) \cdot \exp[-0.25 \cdot (2 \cdot z_r - 1)] \cdot [\cos(\pi / a \cdot (2 \cdot z_r - 1))]$	0.39	$0.5 < z_r$
	for $\lambda = 20.3$: $\varepsilon_{min} = 0.23$ $a = 0.876$		
Cohen and Metzner[146]	$\varepsilon(r) = 1 - (1 - \bar{\varepsilon}_{inf}) \cdot 4.5 \cdot \left(z_r - \frac{7}{9} \cdot (z_r)^2\right)$	n. a.	$z_r \leq 0.25$
	$\varepsilon(r) = \bar{\varepsilon}_{inf} + (1 - \bar{\varepsilon}_{inf}) \cdot 0.3463 \cdot \exp(-0.4273 \cdot z_r) \cdot \cos((2.45 \cdot z_r - 2.2011) \cdot \pi)$	n.a.	$0.25 < z_r < 8$
	$\varepsilon(r) = \bar{\varepsilon}_{inf}$		$8 < z_r$
Mueller[135]	$\varepsilon(r) = \bar{\varepsilon}_{inf} + (1 - \bar{\varepsilon}_{inf}) \cdot J_0(a \cdot z_r) \cdot \exp(-b \cdot z_r)$	0.365	$\lambda \geq 2.02$
	with $a = 7.45 - \frac{3.15}{\lambda}$ $b = 0.315 - \frac{0.725}{\lambda}$	-	$2.02 \leq \lambda \leq 13.0$
	or $a = 7.45 - \frac{11.25}{\lambda}$ $b = 0.315 - \frac{0.725}{\lambda}$	-	$\lambda \geq 13.0$
Bey and Eigenberger[147]	$\varepsilon(r) = \varepsilon_{min} + (1 - \varepsilon_{min}) \cdot \left(\frac{z_r}{z_{min}} - 1\right)^2$	-	$\frac{z_r}{z_{min}} - 1 \leq 0$
	$\varepsilon(r) = \bar{\varepsilon}_{inf} + (\varepsilon_{min} - \bar{\varepsilon}_{inf}) \cdot \exp\left[-0.1 \cdot \left(\frac{z_r}{z_{min}} - 1\right)\right] \cdot \left[\cos\left(\pi / 0.876 \cdot \left(\frac{z_r}{z_{min}} - 1\right)\right)\right]$	0.375	$0 < \frac{z_r}{z_{min}} - 1$
	for $\varepsilon_{min} = 0.24$ $z_{min} = \frac{\lambda}{2} \cdot \left(1 - \sqrt{1 - \frac{2}{\lambda}}\right)$		
Giese[148]	$\varepsilon(r) = \bar{\varepsilon}_{inf} \cdot (1 + 1.36 \cdot \exp(-5.0 \cdot z_r))$	-	-
Vortmeyer and Schuster[149]	$\varepsilon(r) = \bar{\varepsilon}_{inf} \cdot \left(1 + \frac{1 - \bar{\varepsilon}_{inf}}{\bar{\varepsilon}_{inf} \cdot \exp(1)} \cdot \exp(1 + z_r)\right)$	-	-
Suzuki et al[138]	$\varepsilon(r) = \bar{\varepsilon}_{inf} + a \cdot \exp(-b \cdot {z_r}^c) \cdot \cos\left(2 \cdot \pi \cdot {z_r}^d\right)$	n.a.	$\lambda \geq 4.5$
	$a = 0.018 \cdot \ln(\lambda) + 0.483$; $b = 0.312 \cdot \ln(\lambda) + 0.58$; $c = 0.2061 \cdot \ln(\lambda) + 0.128$; $d = -0.033 \cdot \ln(\lambda) + 1.177$		

Schneider and Rippin[102] evaluated the radial locations of the minima and maxima of their own data and those from Benenati and Brosilow[105] and Goodling et al[107] depending on λ. It was found that the locations of the extrema are independent of λ in the tested range (2.5-15), so that the maxima occur at 1.00, 1.86, 2.75, 3.63, and 4.50 sphere diameters from the tube wall. Except for the very first maximum, the period of oscillation appears constant with 0.86-0.88 sphere diameters between consecutive minima and maxima. For validation, the detected maxima positions are marked as dotted lines in Figure 4 showing a great consensus, with the gathered experimental data.

Derived correlations

The above-described experiments led to a selection of empirical correlations being derived to describe the tangentially and axially averaged radial porosity profile, complemented by some (semi-)analytical models. A comprehensive selection of correlations are shown in Table 3. These can generally be classified into the following categories: (a) exponential decay functions,[144,148–152] which completely ignore the oscillation close to the wall; (b) damped oscillatory functions, combining a cosine oscillation with an exponential decay[20,110,145–147] or by using a Bessel function of zero order[135,153,154]; (c) scaleable approaches, that take λ-specific differences

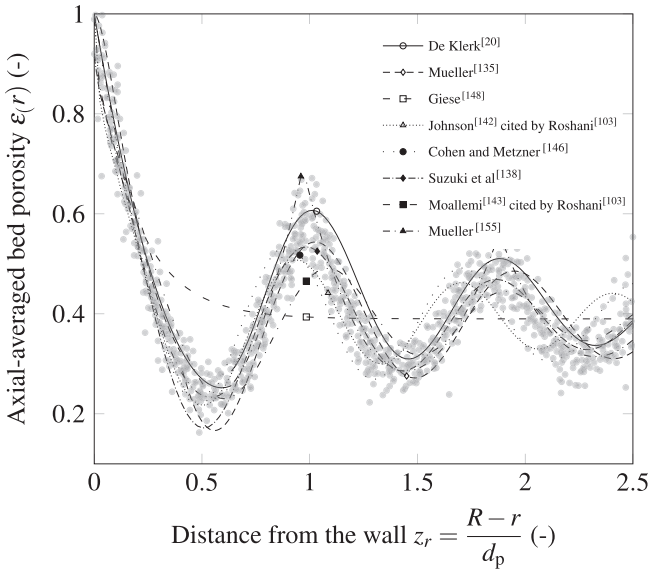

FIGURE 5 Comparison of anonymized experimental radial void distribution data $\epsilon(r)$ obtained with $\lambda > 5.0$ and a selection of empirical and semi-analytical correlations as presented in the literature[20,103,135,138,142,143,146,148,155]

into account[135,138,155]; and (d) statistical sphere centre re-estimations based on experimental radial porosity profiles with subsequent re-calculation of the radial porosity distribution.[33,156–159] This last approach was adopted for $\lambda < 2$ where the sphere locations can be expressed analytically assuming a regular packing arrangement based on λ-dependent unit cell considerations.[160] However, while actually not being a correlation but an inconvenient mathematical approach, it becomes obsolete when sphere centres are determined as experimental output.

Herein, Martin,[145] Chandrasekhara and Vortmeyer,[144] Vortmeyer and Schuster,[149] and Johnson[142] used the data of Benenati and Brosilow[105] to derive their correlations. Cohen and Metzner[146] averaged the experimental data of Roblee et al[104] and Ridgway and Tarbuck.[137] De Klerk[20] and Bey and Eigenberger[147] incorporated a larger selection of existing experimental data. However, the calculation of minima position z_{min} as proposed by Bey and Eigenberger[147] is questionable; for a $\lambda < 2$ no results can be obtained and for $\lambda = 2$, the minima position is at one particle diameter from the wall. The position value decreases with increasing λ approaching 0.5 for infinite λ. Replacing z_{min} with a constant 0.5 is more realistic and in accordance with other results. Doing so, this equation becomes similar to one by Martin.[145]

For comparison, a selection of correlations are plotted for a specific tube-to-particle diameter ratio $\lambda = D/d_p = 5$ as displayed in Figure 5 with the anonymized experimental data taken from Figure 4. Here, only data for packed-beds with $\lambda > 5$ are considered, as packings with lower λ behave significantly different, and do not seem to be representable by current correlations.[161]

While a good consensus among experimental data exists in regard to amplitude and period of the radial void distribution, most empirical correlations struggle to project in particular the correct oscillation period which becomes evident at higher z_r. Only the semi-analytical correlation of Mueller[155] trying to describe the obtained radial void distribution behaviour with a string of parabolas rather than a damped cosine function can correctly reproduce the oscillation period and amplitude of the used data pool. This may be explained with the known inconsistent oscillation period, where the first period is 1.00 and the following periods are around 0.87.[102] The slight overprediction at $z_r < 0.5$ of the Bessel function proposed by Mueller[135] and queried by Theuerkauf et al[161] can be decreased using a recently published functional improvement.[153]

Some experimental procedures result in the provision of sphere centre points rather than directly in the void size distribution. From the centre point coordinates and the sphere's dimensions, axial and radial porosity profiles can be calculated by cutting imaginary plane and cylindrical slices through the mathematically reconstructed spheres.[155,162–166] These slices may have a designated thickness characterizing the volume-based method or not, resulting in the area-based method.

In summary, a wide selection of experimental methods are known for the determination of the tangentially and axially averaged radial porosity distribution, a key parameter for the evaluation of packing structure, though most come with unsatisfactory accuracy for a single measurement. However, when gathering all available literature data regarding packings of spheres into one plot, an impressive consensus can be seen. This consensus cannot be reproduced by most available correlations, especially regarding the oscillation period.

2.2.3 | Pore size and shape

Characterizing the size and shape of the voids within a packed-bed is rather challenging, as pores are non-circular and irregularly converge, diverge, and intersect.[21]

The void size and distribution characterization were first performed in a 2D analytical setup, packing mono-sized circles[167]and later size-distributed circles.[168] The obtained models were then transformed into 3D packings of mono-sized spheres, typically investigated in sliced, solidified packings by image analysis showing circles of different sizes.[114,169] However, several different definitions of pore size exist: Alonso et al[167,169] define the void size as the probability of finding a circle (2D) or sphere

(3D) having a certain diameter completely fitting into a void (no particle intersection), whereas Gotoh et al[170] search for spheres of certain diameter not overlapping with solid sphere centres allowing particle intersections. Moreover, the diameter of void spheres with centres equidistant from four particle centres may be searched.[171,172] Besides spherical void representations, the void size may be calculated by arbitrarily setting a point into the void of a packed-bed and measuring the distance in the axis directions to the next solid boundary.[173] This allows a separate void characterization in the radial and axial directions.

Du et al[114] investigated the pore size and pore size distribution. Although using non-uniform natural packings, the general trends are clear. The larger the particles, the larger the voids while the breadth of distribution is unaffected. The lower the porosity, the smaller the voids and the higher the sphericity of the particles, the broader the distribution.

Pore shapes within packed-beds of random spheres are considered to have distorted tetrahedral and octahedral shape commonly used to describe regular packing arrangements and crystal unit cells.[171] A detailed classification of pore shapes was for instance done by Frost.[172] The mean packing configuration and thus the void shape can be related to the radial distribution function. Configurational entropy can be derived to describe the structural randomness of packings.

In summary, pores have been evaluated rarely; however, no clarity exists in regard to the definition of the pore size measure and the actual necessity of evaluation.

2.2.4 | The thickness effect (influence of the tube height-to-particle diameter ratio)

The influencing effect of the confining base (and top) plate analogous to the wall effect was first addressed by Wadsworth[39] (cited by Haughey and Beveridge[21]) noting that the coordination number decreased from the second to the eighth layer, expressed as the tube height-to-particle diameter ratio $\kappa = H/d_p$ of the packing, indicating a decreasing order. Furthermore, Haughey and Beveridge[21] mention that the first plane layer is found to be perfectly regular. With decreasing distance, however, the distinct layers disappear due to increasing sphere placement options causing an increased amount of randomness.

The thickness effect was further investigated by several research groups[28,49,103,111,113,120,126,128,174] resulting in various recommendations in regard to the minimal packing height that is required to neglect the thickness effect. It was repeatedly shown that at least the bottom plate has an effect similar to that of the surrounding confinement, reaching 4-5 particle diameters into the tube.[120,126]

The most comprehensive study so far regarding the influence of packing height was presented by Zou and Yu[175] investigating the mean porosity by systematically varying κ from 2.5-100. A sharp decrease in porosity is found by increasing κ from 2.5 to around 15 ($\Delta\bar{\varepsilon} = 0.06$). From there on, a slight linear decrease can be observed ($\Delta\bar{\varepsilon} = 0.03$). The obtained results are displayed in Figures 6 and 7. As a consequence, there are two options in order to study packings independently from the top and bottom effects: either a κ large enough to ensure that the effects of the top and bottom are negligible needs to be selected, which is according to their data $\kappa > 20$; or the top and bottom fraction need to be cut away completely.

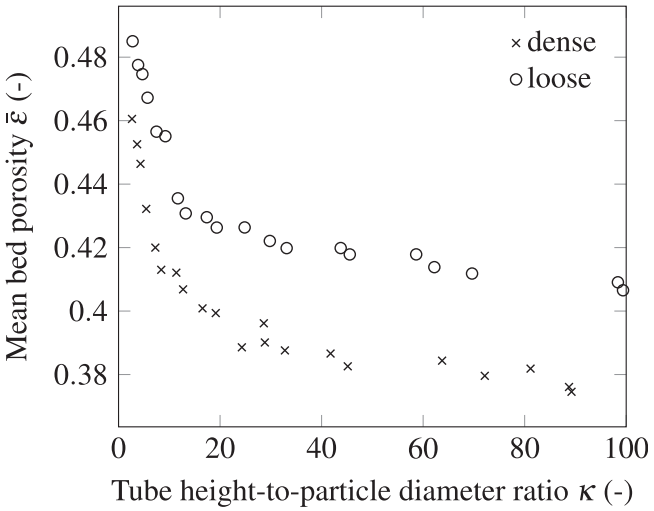

FIGURE 6 Influence of packing height-to-particle diameter ratio κ on the overall bed porosity $\bar{\varepsilon}$ as of Zou and Yu[175] for a dense and a loose random packing arrangement

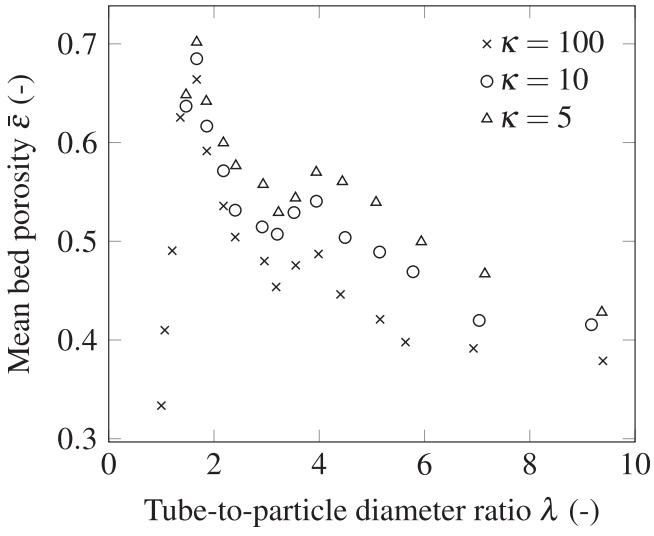

FIGURE 7 Influence of both λ and κ on the overall bed porosity $\bar{\varepsilon}$ for a dense packing arrangement as of Zou and Yu[175]

The thickness effect can also be derived from the axial porosity profiles. Starting from the container's bottom, axial porosity profiles show a similar damped oscillating trend as the radial porosity profiles for the first 3-5 particle diameters. This is then reduced to a noisy constant bulk porosity value throughout the bulk of the packing, before porosity variations increase again when reaching the top of the packing. Only rarely do experimental studies discuss the axial porosity profiles, such as Reimann et al[49] for packings with large λ and Du Toit[162] presenting the recalculated axial porosity profiles of Mueller's[135] data. Only recently, Du Toit[176] presented profiles for packings of $\lambda < 2$ showing a very regular arrangement of particles in the axial direction. However, the axial porosity distribution is a measure of the consistency of the packed bed along the tube height and should therefore be at least included as an illustration in future research work.

2.2.5 | Tube-to-particle diameter ratio

Despite the detailed information local porosity distributions may offer, in some applications and for a general overview it is frequently sufficient to only know the globally averaged bed porosity $\bar{\varepsilon}$. The reduced information is remendied by significantly easier experimentation and thus availability of large data sets. Especially in applications of large λ and κ, where the influence of the confinement surfaces (eg, wall and bottom) is neglectable, the averaged bed porosity may be the primary structural parameter.

Experimental

The most commonly used methods to determine the mean bed porosity are the water displacement method,[112,174,177–180] determining the volume of water needed to completely fill the voids of a packing, and the weighing method,[181,182] which simply weighs all packed-bed particles and determines the void volume via the particle density. The water displacement method is challenging in regard to the elimination of air pockets, the proper determination of the meniscus level, and the pre-soaking of the porous particles. It is of further importance which packing mode is selected; it is therefore thoroughly discussed in section 2.2.6.

Results collected from the literature

The known experimental average bed porosity data depending on the tube-to-particle diameter ratio λ has been summarized in Figure 8. A clear trend and a good consensus of data points can be seen. According to this, the mean packed-bed porosity increases sharply before reaching a global maximum around $\lambda \approx 1.7$, followed by a sharp decrease until reaching $\lambda \approx 2$, and hereinafter flattens out until $\lambda \approx 10$. Besides the clear global maximum, further extrema, especially a minimum at $\lambda = 3.0$ and two possible maxima around $\lambda = 2.7$ and $\lambda = 3.7$, are at least indicated by the given data. In this low-λ range, the possible packing arrangements of spheres in very thin containers significantly affect the porosity. While for $\lambda < 2$ no two spheres fit next to each other into the container, a very regular packing arrangement is obtained and may be described using unit cell considerations. The original results by Govindarao et al[160] have recently been upgraded by Du Toit.[176] Additionally, Guo et al[200] thoroughly investigated packings of $2 < \lambda < 3$ using an analytical approach and experiments. The optimal packing size for integral sphere layers at low λ was studied by McGeary.[192] These theoretically obtained

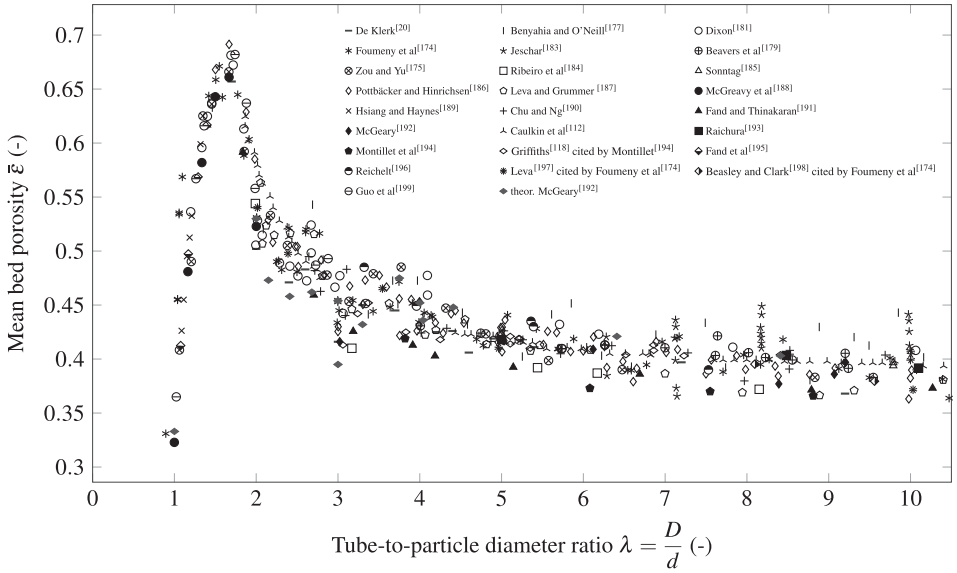

FIGURE 8 Summary of experimental literature results for the average bed porosity $\bar{\varepsilon}$ when varying the tube-to-particle diameter ratio λ for smooth spheres[20,112,118,174,175,177,179,181,183–199]

results are added to Figure 8 and the following structural characteristics were identified for the $\lambda = 2$-5 region. For a sphere number up to five per layer, only one ring can be formed inside the container. One inner sphere fits into a complete ring of 5-7 spheres (making 6-8 spheres in total), three inner spheres can be placed into an inner ring of 6-9 spheres (making 9-12 spheres in total). From there on, an orthorhombic arrangement is assumed where the innermost ring has four, the next one 10, and if needed the following 17, 24, 31, and so on. Based on these findings, a sharp porosity minimum at $\lambda = 3.0$ and a subsequent maximum at $\lambda = 3.75$ can be identified. A smaller minimum/maximum pair can be found at $\lambda = 2.41$ and $\lambda = 2.68$ and for $\lambda = 4.04$ and $\lambda = 4.41$. It must be noted that for $\lambda = 3.0$ two configurations exist comprising either 6 or 7 spheres. While the seven-sphere arrangement causes the minimum, the six-sphere arrangement fits perfectly into the generally assumed decreasing function. Furthermore, De Klerk[20] mentions bed voidage values higher or lower than expected for tube-to-particle diameter ratios 2.4, 3.0, and 4.6. Moreover, for a diameter ratio of 3.0, two data points were recorded, deviating considerably from the average to higher values. This last finding is in agreement with the study of McGeary.[192]

Derived correlations

Based on the obtained experimental data, a large number of correlations regarding the influence of tube-to-particle diameter ratio on the average packing porosity were derived. A comprehensive summary can be found in Table 4. For comparison, these correlations were plotted in Figure 9 together with the anonymized literature data as displayed in Figure 8.

While the given correlations fit the overall scope of the experimental data well, they vary in regard to the infinite bed porosity obtained for $\lambda \to \infty$, which is strongly dependent on the packing method and material characteristics. From the considered correlations, the one presented by Foumeny et al[174] represents the overall trend best. It must be noted that no further extrema than the obvious global peak are considered in the known correlations. Only Zou and Yu[175] included a detected maximum at around $\lambda = 4.0$ into their piecewise defined correlation.

TABLE 4 Overview of known wall effect correlations

Source	Formula	$\bar{\varepsilon}_{inf}$	Scope
Carman[201]	$\bar{\varepsilon} = 1 - \frac{2}{3}\cdot\left(\frac{1}{\lambda}\right)^3 \cdot \frac{1}{\sqrt{\frac{2}{\lambda}-1}}$	-	$1 < \lambda \leq 1.866$
Aerov[202]	$\bar{\varepsilon} = \bar{\varepsilon}_{inf} + \frac{0.07}{\lambda} + \frac{0.54}{\lambda^2}$	0.39	$\lambda \geq 2$
Sonntag[185]	$\bar{\varepsilon} = \bar{\varepsilon}_{inf} + (1-\bar{\varepsilon}_{inf})\cdot\frac{0.526}{\lambda}$	0.359	$10 \leq \lambda \leq 30$
Jeschar[183]	$\bar{\varepsilon} = \bar{\varepsilon}_{inf} + \frac{0.34}{\lambda}$	0.375	$6.25 \leq \lambda \leq 100$
Ayer and Soppet[182]	$\bar{\varepsilon} = \bar{\varepsilon}_{inf} + 0.216\cdot\exp(-0.313\cdot\lambda)$	0.365	$3 \leq \lambda \leq 32$
Beavers et al[179]	$\bar{\varepsilon} = \bar{\varepsilon}_{inf}\cdot\left[1 + \frac{2}{\lambda}\cdot\left(\frac{\bar{\varepsilon}_w}{\bar{\varepsilon}_{inf}} - 1\right)\right]$	0.368	$4 \leq \lambda < 45 \quad \bar{\varepsilon}_w = 0.476$
Froment and Bischoff[203]	$\bar{\varepsilon} = \bar{\varepsilon}_{inf} + 0.073\cdot\left[1 - \frac{(\lambda-2)^2}{\lambda^2}\right]$	0.38	n.a.
Griffiths[118] cited by Roshani[103]	$\bar{\varepsilon} = \bar{\varepsilon}_{inf} + \frac{0.035}{(\lambda-3.5)^{0.27}}$	0.38	$\lambda > 3.5$
Dixon[181]	$\bar{\varepsilon} = \bar{\varepsilon}_{inf} + \frac{0.05}{\lambda} + \frac{0.412}{\lambda^2}$	0.40	$\lambda \geq 2$
Fand and Thinakaran[191]	$\bar{\varepsilon} = \bar{\varepsilon}_{inf} + \frac{0.151}{\lambda-1}$	0.36	$2.033 \leq \lambda < 40$
Fand and Thinakaran[191]	$\bar{\varepsilon} = 1.8578 - 0.6649\cdot\lambda$	-	$1.866 \leq \lambda < 2.033$
Foumeny et al[174]	$\bar{\varepsilon} = \bar{\varepsilon}_{inf} + 0.254\cdot\frac{\lambda^{-0.923}}{\sqrt{0.723\cdot\lambda-1}}$	0.383	$1.866 \leq \lambda < 22$
Mueller[135]	$\bar{\varepsilon} = \bar{\varepsilon}_{inf} + \frac{0.220}{\lambda}$	0.365	$\lambda \geq 2.02$
Zou and Yu[175]	$\bar{\varepsilon} = \bar{\varepsilon}_{inf} + 0.002\cdot\left[\exp\left(\frac{15.306}{\lambda}\right) - 1\right]$	0.372	$3.95 \leq \lambda < 35$
Zou and Yu[175]	$\bar{\varepsilon} = 0.681 - \frac{1.363}{\lambda} + \frac{2.241}{\lambda^2}$	-	$1.866 \leq \lambda < 3.95$
De Klerk[20]	$\bar{\varepsilon} = \bar{\varepsilon}_{inf} + 0.35\exp(-0.39\cdot\lambda)$	n.a.	$2 \leq \lambda < 20$
Benyahia and O'Neill[177]	$\bar{\varepsilon} = \bar{\varepsilon}_{inf} + \frac{1.74}{(\lambda+1.14)^2}$	0.39	$1.5 \leq \lambda < 50$
Puschnov[204]	$\bar{\varepsilon} = 12.6\cdot\lambda^{6.1}\cdot\exp(-3.6\cdot\lambda)$	-	$1 \leq \lambda < 2.4$
Puschnov[205]	$\bar{\varepsilon} = \bar{\varepsilon}_{inf} + \frac{1}{\lambda^2}$	-	$2 \leq \lambda < 20$
Cheng[206]	$\bar{\varepsilon} = \left[\frac{1}{\left(0.8\cdot(\lambda-1)^{0.27}\right)^3} + \frac{1}{\left(\bar{\varepsilon}_{inf}\cdot\left(1+(\lambda-1)^{-1.9}\right)\right)^3}\right]^{-1/3}$	0.38	$1 \leq \lambda < 100$
Ribeiro[184]	$\bar{\varepsilon} = \bar{\varepsilon}_{inf} + 0.917\exp(-0.824\cdot\lambda)$	0.373	$2 \leq \lambda < 19$

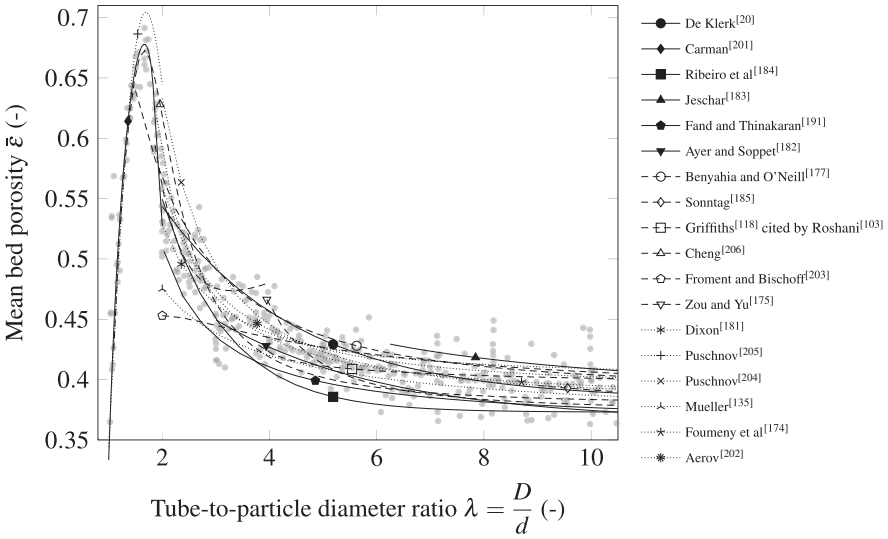

FIGURE 9 Anonymized experimental literature data as displayed in Figure 8 and known correlations regarding the influence of tube-to-particle diameter ratio λ on the mean bed porosity $\bar{\varepsilon}$ of smooth spheres[20,103,118,135,174,175,177,181–185,191,201–206]

In summary, a large data pool is available relating the average bed porosity to the tube-to-particle diameter ratio of a packing. These data can be well represented by a large selection of known correlations, except some details such as local extrema.

2.2.6 | Influence of packing mode

Haughey and Beveridge[20,21] determined four particular methods of bed formation. The associated porosity ranges are based on a range of literature data and are valid when wall effects are insignificant ($\lambda \to \infty$). The modes comprise:

1. Very loose random packing ($\bar{\varepsilon}\approx 0.44$) obtained by settling a fluidized bed, by sedimentation, or by inversion of the bed container.
2. Loose random packing ($\bar{\varepsilon}\approx 0.40-0.41$) obtained by letting the spheres roll individually into place, individual hand packing, or by dropping the spheres as complete loose mass.
3. Poured random packing ($\bar{\varepsilon}\approx 0.375-0.391$), obtained by pouring particles into the container.
4. Close random packing ($\bar{\varepsilon}\approx 0.359-0.375$) obtained by vibrating, shaking, or tapping of the container.

Thus, compared to regular packings where the mean bed porosity varies between 0.26 and 0.48 depending on their arrangement (see Table 1), random packings may take on values between 0.36 (Random Close Packing(RCP)) and 0.44 (Random Loose Packing (RLP))[21] when not confined. A comprehensive overview of experimental data sorted by packing mode based on the above classification was collected by Roshani.[103] Another packing state, the so-called maximally random jammed state (MRJ), evolved in physical contexts which are mathematically precise equivalents to the RCP state.[207,208]

The upper limit, so-called RLP, was for example studied by Onoda and Leiniger[209] in settling experiments under zero gravitational force and in shear-cell experiments with glass spheres. A value of up to 0.445 ± 0.005 was obtained as an upper limit. Furthermore, it was repeatedly shown that packed-beds generated without significant effort to form extra loose or dense beds show packing porosities around 0.38-0.39.[174,186,210] Consequently, this small range is generally accepted as the standard packing porosity of a sphere packing.

Regarding the evaluation of the porosity of the densest possible sphere packing in the absence of global order, Susskind and Becker[211] removed the air from balloons filled with spherical particles. For a typical packing a value of $\bar{\varepsilon}_{\text{inf}} = 0.362$ could be obtained. This value was lowered to $\bar{\varepsilon}_{\text{inf}} = 0.348$ by rigorous vibration. However, Bernal and Finney[212] remarked that even when using a non-rigid balloon, confinement effects cannot be neglected and recalculated the data to a RCP porosity of around 0.36.[38,43] Nonetheless, using appropriate experimental conditions, vibrated packed-beds may adopt a global order, allowing porosities slightly below the RCP limit.[49]

In-detail studies on packing densification were performed using vibration[174,213–217] or tapping.[218,219] Typically, packed-bed porosity decreases until the densification is saturated.[213,215,217,219] Optimal vibration frequency and amplitude settings are required to gain the densest packings (cf.[213–215,220]). Furthermore, interparticle diffusion during vibration was investigated.[215]

Besides vibration, the achieved packing densification by tapping n taps and a certain relaxation time τ can be described as below.[219,221,222]

Sequential addition compared to shaking was done by Baker and Kudrolli.[220] Another filling method called sock filling was performed by Bazmi et al[223] Afandizadeh and Foumeny[28] investigated three different packing methods: fast pouring, slow pouring, and the so-called snow storm filling,[224] where the packing material is passed over wire meshes to interrupt its free fall inside the tube. The mean bed porosity decreased for longer filling times and a filling speed of 0.5-5 mm bed length per second is suggested to obtain more reproducible packings. Moreover, Macrae and Gray[225] investigated the influence of particle drop height, deposition intensity, and filling rate (particle number per filling time). It was found that the packing porosity decreases with a higher drop height before reaching a final value, with a reduced particle filling rate and lower deposition intensity.

Besides the influence of densification on the average bed density, structural studies reveal that an increase in oscillation amplitude and a decrease in the oscillation period affect the radial porosity distribution[49,226] along with the increased bed densification. The more ordered a packing gets, the more distinct the parabolic shape of the radial void distribution gets. Very ordered packings form tiny intermediate parabolas so that the radial porosity distribution resembles a chain of large and small parabolas.[33,49]

The influence of packing formation in fluids other than air was also studied. Staněk and Eckert[120] compared particle damping in air and ethanol during the packed-bed formation, finding a decreased mean porosity when damped in a liquid. Furthermore, Chu and Ng[190] packed the spheres in water. Feng and Yu[67] found an increasingly damped packing behaviour (resulting in higher porosities) using wetted particles with increasing liquid content. Regarding liquid characteristics, surface tension alters the packing structure but small variations in viscosity had no effect.

In summary, the packing mode is one of the most crucial parameters regarding the packing structure and average porosity. Some explicit packing modes have been identified and allocated to certain porosity ranges. Furthermore, packing densification was studied by several research groups leading to lower overall bed porosities and higher packing order.

2.3 | Influence of particle shape

Industrially used shapes comprise cubes and hollow cubes, four-hole cylinders, hollow cylinders with a single bridge or cross web and grooved cylinders, and a selection of saddles and ring shapes.[28,177,227–229] In experiments, shapes comprising cylinders,[114,124,230,231] Pall rings,[124] Raschig rings[232] and Hama beads,[124] prisms,[230,231] ellipsoids,[231–233] trilobes,[218,223] cubes,[114,231] polyhedrons,[232,234] and platonic shapes[220,235] were investigated.

In order to compare shapes other than spheres, a characteristic diameter is used, typically the Sauter diameter $d_{p,s}$ or the diameter of a volume-equivalent sphere $d_{p,v}$:

$$d_{p,s} = 6 \cdot \frac{v_p}{a_p} \tag{2}$$

$$d_{p,v} = \left(\frac{6 \cdot v_p}{\pi} \right)^{1/3} \tag{3}$$

Further equivalent diameters (see Allen[236] for a comprehensive list) based on physical properties are the equivalent sphere diameter having the same sedimentation velocity as the investigated particle $d_{p,w}$ and the equivalent sphere diameter having the same resistance to flow $d_{p,d}$.

The true sphericity Ψ_W as defined by Wadell[237] is a frequently used shape factor to describe shape variations in regard to spheres:

$$\Psi_W = \frac{\pi^{1/3} \cdot (6 \cdot v_p)^{2/3}}{a_p} \tag{4}$$

This parameter was occasionally used to correlate shape and packing porosity at infinite λ. Table 5 gives an overview of the obtained correlations and Figure 10 shows a selection of experimental data points and plotted correlations. In general, there is for an infinite packed bed a tendency towards a larger packing porosity, but no clear trend nor a single all inclusive correlation can be deduced. However, it was not possible to diversify this plot for different packing modes or packing materials used by the researchers, which have a strong influence on the packing porosity obtained for infinite packed beds. According to Zou and Yu,[231] three branches can be identified in the sphericity-porosity plot corresponding to elongated cylinders (upper branch), flat disks (lower branch), and all other shapes, especially hollow cylinders and saddles in between these two borders. Still, the sphericity alone is obviously not capable of describing or predicting the packing porosity of an arbitrarily shaped particle.

TABLE 5 Overview of shape-porosity correlations based on the sphericity

Source	Formula	Scope and parameters	Shapes	No. of datapoints
Benyahia and O'Neill[177]	$\bar{\varepsilon}_{inf} = 0.1504 + \frac{0.2024}{\Psi_W}$		Sphere, cylinder, hollow cylinder, 4-hole cylinder	9
Brown[227]	$\bar{\varepsilon}_{inf} = \bar{\varepsilon}_{inf,s}^{1.785\cdot\Psi_W^{1.585} - 0.785\cdot\Psi_W^{4.897}}$	$\bar{\varepsilon}_{inf,s} = 0.47$ (loose), 0.36 (dense) or 0.42 (mean)	Spheres, cylinders, hollow cylinders, saddles	29
Yu and Standish[228]	$\bar{\varepsilon}_{inf} = \bar{\varepsilon}_{inf,s}^{15.521\cdot\Psi_W^{3.853} - 14.521\cdot\Psi_W^{4.342}}$	$\bar{\varepsilon}_{inf,s} = 0.40$ (loose), 0.36 (dense) or 0.38 (mean)	Spheres, cylinders, hollow cylinders, saddles	Data of[238–240]
Zou and Yu[231,241]	$\bar{\varepsilon}_{inf} = \exp\left(\Psi_W^{5.58}\cdot\exp(5.89\cdot(1-\Psi_W))\cdot\ln(0.40)\right)$	Dense packing: 6.74, 8.00, 0.36	Cylinders, disks, balls, beads, beans, lentils, cubes, prisms	36
	$\bar{\varepsilon}_{inf} = \exp\left(\Psi_W^{0.6}\cdot\exp\left(0.23\cdot(1-\Psi_W)^{0.45}\right)\cdot\ln(0.40)\right)$	Dense packing: 0.63, 0.64,1.0, 0.36		
Warren et al[242]	$\Psi_W = 0.079 + 0.831\cdot(1-\bar{\varepsilon}_{inf}) + 1.53\cdot(1-\bar{\varepsilon}_{inf})^3$			
Lanfrey et al[229]	$\Psi_W = \sqrt{\frac{1.23}{T}\cdot\frac{(1-\bar{\varepsilon}_{inf})^{4/3}}{\bar{\varepsilon}_{inf}}}$	Tortuosity $T = 2.12$ in mean, between 1-3 in general	Berl, Intalox and Torus saddles, Raschig, Pall and Ralu Rings, different material and size	> 100
Parkhouse and Kelly[243]	$\bar{\varepsilon}_{inf} = 1 - 2\cdot\ln(a_1)/a_1$ with $\Psi_W = 2.621\frac{a_1^{2/3}}{1+2\cdot a_1}$	$a_1 > 7$	Elongated cylinder	4
Blouwolff and Fraden[244]	$\bar{\varepsilon}_{inf} = \frac{5.4}{a_1}$ with $\Psi_W = 2.621\frac{a_1^{2/3}}{1+2\cdot a_1}$		Elongated cylinder, different material	6
Rahli[245] cited by Novellani et al.[246]	$\bar{\varepsilon}_{inf} = 1 - \frac{11}{\frac{\pi}{2\cdot a_1} + 6 + 2\cdot a_1}$ with $\Psi_W = 2.621\frac{a_1^{2/3}}{1+2\cdot a_1}$	-	Elongated cylinder	

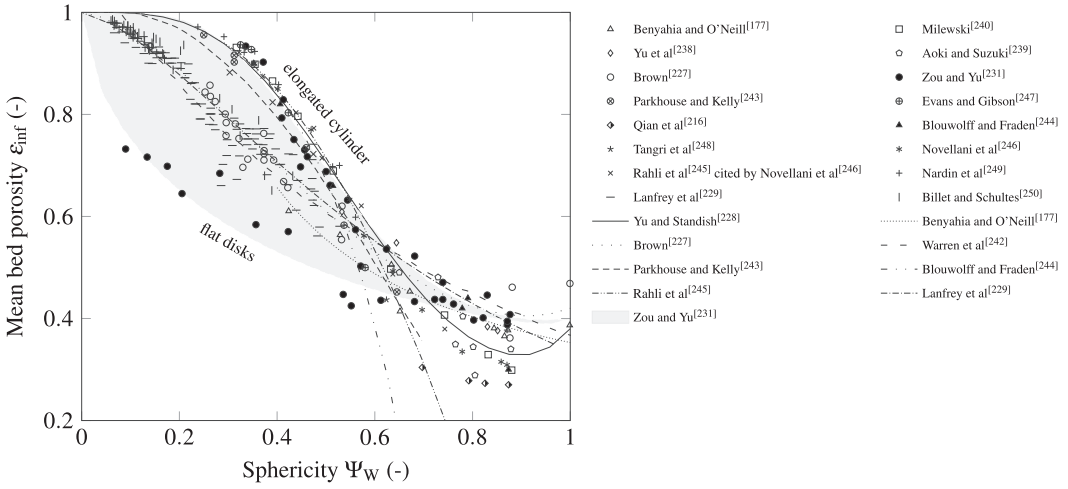

FIGURE 10 Experimental literature data regarding the sphericity Ψ_W dependent evaluation of packed-bed bulk porosity ε_{inf}[177,216,227–229,231,238–240,242–250]

As a second shape parameter, Lanfrey et al[229] utilized the tortuosity T together with the sphericity in order to estimate packed-bed porosities. The tortuosity is typically defined as the ratio of the actual fluid flow path and the packing height. It reaches values around 1.4 = 1.5 for spheres[251,252] and may be correlated to the packing porosity.[253–257] Unfortunately, a large number of data points of the elongated cylinders displayed in Figure 10 would be allocated a tortuosity value below unity when applying Lanfrey et al's correlation[229] to Figure 10.

Moreover, Yu and Standish[228] developed a characteristic packing diameter d_{pack} that can be used together with the sphericity to describe packings of arbitrary shapes or size variations. This packing diameter is defined as the diameter of a sphere that leads to a maximum packing porosity in a binary mixture with the investigated shape. This attempt is inconvenient as it requires a large number of experiments for the determination of a single characteristic diameter and was tested for a small selection of convex shapes only[228,231]:

$$\frac{d_{p,v}}{d_{pack}} = \Psi_W^{2.785} \cdot \exp[2.946 \cdot (1 - \Psi_W)]. \quad (5)$$

Other shape factors are known in the context of characterizing undesignated granular material, as for instance the empirical Heywood factor.[236,258,259] Here, flatness m and elongation n of a particle are defined and related to the shape's sphericity[231]:

$$\Psi_W = \frac{2.418}{(m \cdot n^{-2})^{1/3} + (m^{-2} \cdot n)^{1/3} + (m \cdot n)^{1/3}}. \quad (6)$$

Moreover, a correlation of the sphericity and the Hausner ratio known from powder beds and describing the compressibility of a packing was found.[241,260,261] A tendency of a larger Hausner ratio and thus packing compressibility was obtained with decreasing shape sphericity but with a large data scatter[231]:

$$H_r = 1.478 \cdot 10^{-0.136 \cdot \Psi_W}. \quad (7)$$

Despite a large number of available randomly packed shapes, only a small selection is studied in further detail. With higher complexity in particle shape, the predictability of the packing structure becomes increasingly elaborate. While a single sphere within a packing can basically be described by two parameters, the centre location and the (characteristic) diameter, a cylindrical shape needs to be further characterized by its orientation (eg, rotation matrix) and a shape factor called aspect ratio defining its height-to-diameter ratio a_1. Further improvement of the simple cylindrical shape is done by cutting a straight axial hole and obtaining a hollow cylinder often called Raschig ring. The list of parameters required to entirely describe this shape is enlarged by a second aspect ratio giving the inner to outer ring diameter a_2. Similarly, an ellipsoid can be described completely by two aspect ratios. Any more complex shape requires a whole set of aspect ratios while any variation in these parameters will presumably affect the packing characteristics (even when keeping other influences like material or packing mode constant). It is still possible to describe the packing of a specific complex shape by performing the relevant studies, but it is hard to predict the performance of an arbitrary shape or even geometrically similar shapes from the obtained results. Thus, experimental studies exist and will be described in the following regarding packing properties for cylinders and rings, although the database is much smaller compared to spheres. A comprehensive list of experimental studies involving shapes other than spheres is presented in Table 6.

The most notable results from this list are summarized in Figure 11 regarding radial void distribution and average bed porosity for equilateral cylinders, non-equilateral cylinders, and hollow cylinders, respectively. It was not possible when comparing the data from the respective plots as was done for spheres, as the data showed significant differences when comparing the data from different research groups. Clustering was thus impossible. Consequently, the reproduced data are selected due to their extent, not their claim of correctness compared to other data sets. However, some general trends may be derived and are discussed in the following.

Equilateral cylinders

The equilateral cylinder is a cylinder with equal height and diameter. Regarding the available radial void distribution of cylinder packings at various tube-to-particle diameter ratios[103] in comparison to a packing of spheres (cf. Figure 11A), similarities in the general oscillatory trend can be seen. However, the amplitude, period and bulk porosity take on slightly different values. Consequently, very similar correlations can be derived, namely Küfner and Hofmann,[110] based on Vortmeyer and Schuster[149]:

$$\varepsilon(z_r) = \bar{\varepsilon}_{inf} \cdot \left(1 - \frac{1 - \bar{\varepsilon}_{inf}}{\bar{\varepsilon}_{inf} \cdot \exp(1)} \cdot \exp(1 + z_r) \cdot \cos(2 \cdot \pi \cdot z_r)\right), \quad (8)$$

Roshani[103]:

$$\varepsilon(z_r) = 1 - 0.695 \cdot (1 - \exp(-1.83 \cdot (z_r)^{0.34}) \cdot \cos(6.65 \cdot (z_r)^{1.08}), \quad (9)$$

and Bey and Eigenberger[147]:

$$\varepsilon(z_r) = \varepsilon_{min} + (1 - \varepsilon_{min}) \cdot (z' - 1)^2 \quad \text{for} \quad z' \le 1$$
$$\varepsilon(z_r) = \bar{\varepsilon}_{inf} + (\varepsilon_{min} - \bar{\varepsilon}_{inf}) \cdot \exp[-0.5 \cdot (z' - 1)] \cdot [\cos(\pi / 0.876 \cdot (z' - 1))] \quad \text{for} \quad 1 < z'$$
$$\text{with} \quad \varepsilon_{min} = 0.275 \quad z' = \left(1.8 - \frac{2}{\lambda}\right) \cdot \left(\frac{R - r}{d}\right). \quad (10)$$

Regarding the average bed porosity as a function of the tube-to-particle diameter ratio in Figure 11B, a very

TABLE 6 Overview of experimental studies relating to the structural analysis of packed-beds of non-spherical particles

Source	Shape	Aspect ratio $1/a_1$	Aspect ratio a_x	λ_v	$\bar{\varepsilon}(\lambda)$	$\epsilon(r)$	$\epsilon(z)$
Giese et al[136]	Cylinder	1	-	9.15	1	1	-
	Hollow cylinder	1	0.75	9.15	1	1	-
	Deformed sphere	-	-	> 10	1	1	-
Benyahia[262]	Cylinder	0.25 to 3	-	3.51-14.04	10	10	10
Caulkin et al[111]	Cylinder	1	-	7.1	1	1	1
	Hollow cylinder	1	0.16-0.47	7.2-7.7	3	3	3
	4-hole cylinder	1	-	7.4	1	1	1
Baker and Kudrolli[220]	Platonic	4-20 faces	-	5 to 7	6	-	-
Baker and Kudrolli[220]	Cylinder	1	-	4.44/9.33	1	1	-
Benyahia and O'Neill[177]	Cylinder	0.76-1.78	-	1.7-26.3	> 10	-	-
	Hollow cylinder	0.38-1.06	Not specified	1.9-14.5	> 10	-	-
	4-hole cylinder	1.14-1.26	Not specified	1.9-8.4	> 10	-	-
Roblee et al[104]	Cylinder	1	-	11.75	-	1	-
	Hollow cylinder	1	0.72	11.75	-	1	-
	Berl saddle	Regular	> 10	-	-	1	-
Sonntag[185]	Cylinder	1	-	11-40	>10	(✓)	-
	Hollow cylinder	1	0.62-0.78	5.6-25	>10	(✓)	-
Lerou and Froment[119]	Cylinder	1	-	5.35	1	1	-
	Hollow cylinder	0.94	0.43	n.a.	1	1	-
Bey and Eigenberger[147]	Cylinder	0.833-3.333	-	5.35	4	-	-
	Hollow cylinder	1	0.44-0.63	3.33-10	4	-	-
Blouwolff and Fraden[244]	Cylinder	0.4-50	-	n.a.	6	-	-
Chikhi et al[230]	Cylinder, prism	0.88-1.4	> 10	-	6	-	-
Comiti and Renaud[263]	Parallelepiped	0.102-0.44	> 10	-	5	-	-
Foumeny and Roshani[178]	Cylinder	0.5-2	-	2-32	> 10	-	-
Foumeny et al[180]	Cylinder	0.5-2	-	2.76-16.67	> 10	-	-
Xie et al[214]	Cube, cuboid	1-4	1-2	5.5-11.5	12	-	-
Xia et al[264]	Ellipsoid	0.51	1	> 10	1	-	-
Wang et al[265]	Ring	n. a.	n. a.	> 10	3	3	-
Zhang et al[226]	Cylinder	1	-	> 10	1	1	-
Lumay and Vandewalle[219]	cylinder	1.67-90	-	n.a.	> 10	-	-
Novellani et al[246]	Cylinder	1.2-50.5	-	n.a.	10	-	-
Man et al[266]	Ellipsoid	1.25:1:0.8	-	6.7-11	5	1	-
Jaoshvili et al[267]	Tetrahedra	reg.	-	n.a.	7	-	-
Parkhouse and Kelly[243]	Cylinder	6.8-143	-	n.a.	-	-	-
Qian et al[216]	Cylinder	0.5-5	-	>10	16	-	-
Zou and Yu[241]	Cylinder	1-100	-	4-40	> 10	-	-
Montillet and Coq[115]	Cylinder	5.3	-	16.3	1	1	-
	Parallelepiped	0.209	-	17.7	1	1	-
Nguyen et al[134]	Cylinder	1.1	-	15	1	1	-
	Trilobe	n.a.	-	24	1	1	-
	Ring	1	0.1 to 0.2	> 10	2	2	-
Wehinger et al[268]	Hexagons	1.1	-	6.3, 4.6	2	2	-

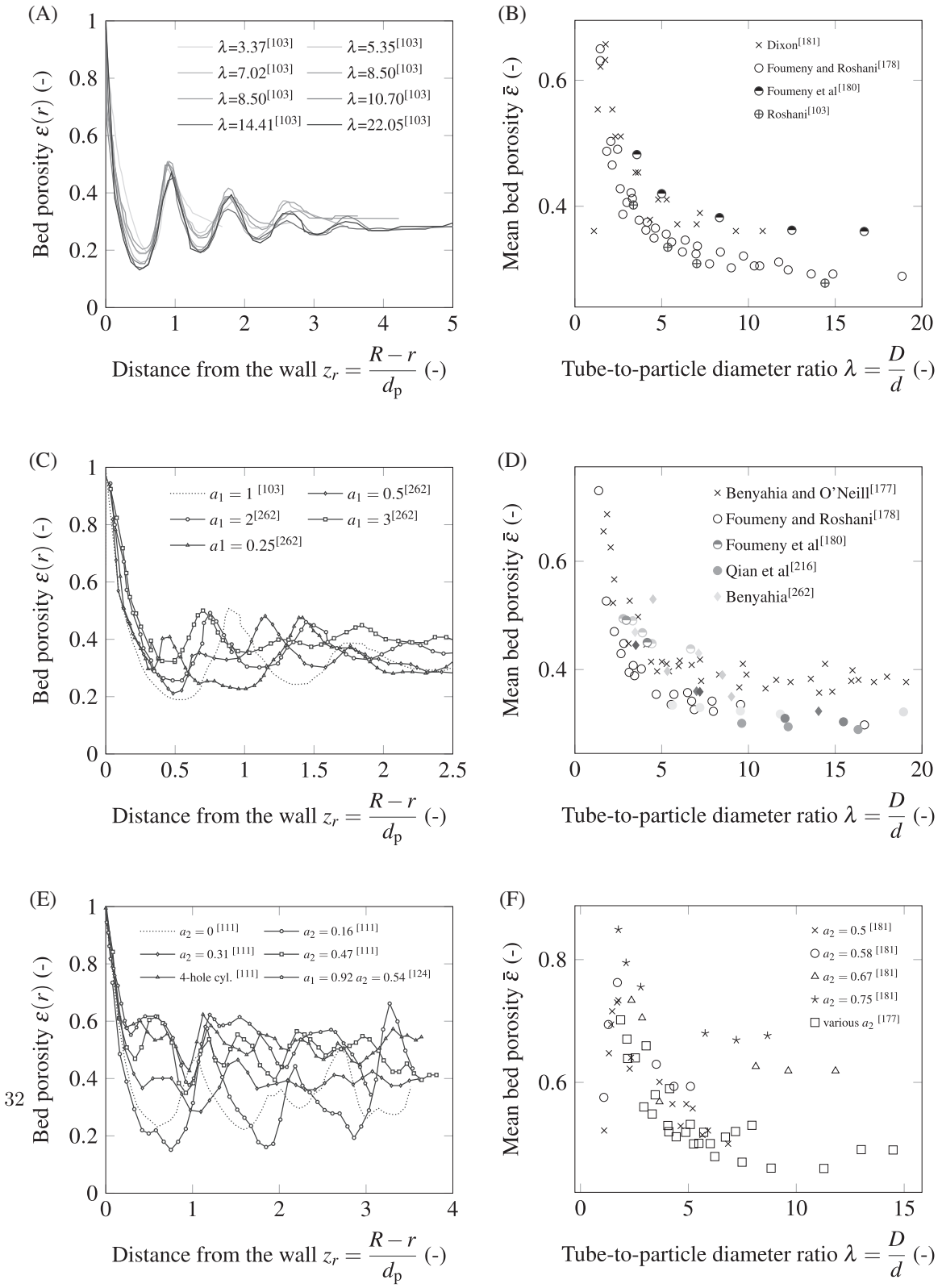

FIGURE 11 Radial porosity distribution $\varepsilon(r)$ for A, equilateral cylinders; C, non-equilateral cylinders; E, hollow cylinders, and average packing porosity -ε for porosity for various cylinder shapes.[103,111,124,177,178,180,181,216,262] A, radial porosity distribution $\varepsilon(r)$ for equilateral cylinders at various tube-to-particle diameter ratios λ.[103] B, mean packing porosity $\varepsilon(r)$ for equilateral cylinders as a function of size ratio λ. C, radial porosity distribution ε(r) for non-equilateral cylinders.[262] D, mean packing porosity $\varepsilon(r)$ for non-equilateral cylinders as a function of size ratio λ. E, radial porosity distribution ε(r) for hollow cylinders.[111] F, mean packing porosity $\varepsilon(r)$ for hollow cylinders as a function of size ratio λ

similar behaviour compared to spheres can be seen: the sharp porosity increase at the beginning, the global maximum, the sharp decrease, and the flattening out after reaching $\lambda = 10$. There is a difference in the significantly larger data scattering, especially at large λ, and the overall smaller porosity. The densest cylindrical packing is found to be 0.27.[216] Further dense packed packings have porosities around 0.3[244] and between 0.28-0.31.[218] Again, correlations were derived basically by adjusting the coefficients of the already known correlations for spheres, namely Dixon[181]:

$$\bar{\varepsilon} = \bar{\varepsilon}_{\text{inf}} + \frac{0.1}{\lambda_v} + \frac{0.7}{\lambda_v^2} \quad \text{with} \quad 1.67 \le \lambda_v \le 20 \quad \bar{\varepsilon}_{\text{inf}} = 0.36 \tag{11}$$

$$\bar{\varepsilon} = 1 - \frac{0.763}{\lambda_v^2} \quad \text{with} \quad \lambda_v \le 1.24, \tag{12}$$

and Foumeny and Roshani[178]:

$$\bar{\varepsilon} = \bar{\varepsilon}_{\text{inf}} + 0.684 \cdot \lambda_{\text{v}}^{-0.85} \cdot \frac{1}{\sqrt{(1.837 \cdot \lambda_{\text{v}} - 1)}} \quad \text{with} \quad \lambda_v \le 1.44 \tag{13}$$

Additionally, particle orientation effects become relevant. The X-ray study of Caulkin et al[124] reveals a particle axis orientation peak for angles of 50-60° to the tube axis, decreasing in both directions. Especially particles orientated at 0-30° are rarely found.

Non-equilateral cylinders

Regarding non-equilateral cylinders, the radial porosity distribution shows a completely different and quite irregular pattern. As displayed in Figure 11C, the peak and minima occurrences do not appear to follow a specific rule, or at least this rule can not be identified with the small amount of available data. This accounts for flat disks as well as for elongated cylinders. However, the overall variance (or amplitude) seems to be smaller compared to equilateral cylinders. Thus, no appropriate correlation could be derived so far to describe the radial void distribution for non-equilateral cylinders.

The average bed porosity as a function of tube-to-particle diameter ratio for selected available data is displayed in Figure 11D. Here, the data appears to follow a similar pattern as observed for spheres and equilateral cylinders. The influence of aspect ratio on the porosity of an infinite bed was already discussed above, where the densest packing was obtained with equilateral cylinders. Regarding confined packings at low tube-to-particle diameter ratios and low cylinder aspect ratio variation between 0.5 and 2, a difference in packing porosity was either too small to differentiate[178,180,241,262] or results indicate a slight influence similar to the porosity of an infinite bed, where packing porosity increases as the aspect ratios move away from unity.[216,262] In Figure 11D, the aspect ratio is displayed as the gray scale of the markers, with a mean gray representing an aspect ratio of 1. However, the deviations between the data sets and the limited number of data per set do not allow a definite conclusion. Nonetheless, some correlations were derived including or explicitly excluding the influence of the aspect ratio comprising Foumeny and Roshani[178,269]:

$$\bar{\epsilon} = \bar{\varepsilon}_{\text{inf}} \cdot \Psi_{\text{W}}^{a} + 0.254 \cdot \Psi_{\text{W}}^{b} \cdot (\lambda_v)^{-0.293 \cdot \Psi_{\text{W}}^{c}} \cdot \frac{1}{\left(0.723 \cdot \Psi_{\text{W}}^{d} \cdot \lambda_{\text{v}} - 1\right)^{0.5}} \quad \text{with} \quad \bar{\varepsilon}_{\text{inf}} = 0.383, \tag{14}$$

and Benyahia and O'Neill[177]:

$$\bar{\varepsilon}_{\text{inf}} = 0.293. \quad \bar{\epsilon} = \bar{\varepsilon}_{\text{inf}} + \frac{1.703}{(\lambda + 0.611)^2} \quad \text{with} \quad \bar{\varepsilon}_{\text{inf}} = 0.373. \tag{15}$$

Hollow cylinders and rings

In order to describe hollow cylinders, a second aspect ratio a_2 of the inner and outer ring diameters is included. A selection of radial porosity profiles obtained from hollow cylinders[111,124] with different aspect ratios a_2 are displayed in Figure 11E. Accordingly, larger values of a_2 result in a significantly higher and smoother porosity distribution. The minima in particular are clearly smoothed compared to solid cylinders. On the contrary, new intermediate maxima of which the height increases as a_2 increases occur. No correlations have been derived so far.

The sparsely available experimental data in the literature of average bed porosity values for different λ and aspect ratios a_2 are summarized in Figure 11F. The general trend is in accordance with solid cylinders and spheres; however, the porosity of an infinite bed increases significantly with increasing a_2. The most comprehensive study in this context was performed by Dixon[181] investigating equilateral hollow cylinders with $a_2 = 0.5$, 0.58, 0.65, and 0.75. As correlation, the calculated solid cylinder base $\bar{\varepsilon}_{\text{sc}}$ Equation (11), corrected with the inner void is used:

$$(1 - \bar{\varepsilon}_{\text{sc}}) = \frac{1 - \bar{\varepsilon}}{f \cdot \left(1 - (a_2)^2\right)}. \tag{16}$$

Regarding interpenetration of hollow cylinders with large holes, a correction f of this correlation for $a_2 > 0.5$ is suggested:

$$f = 1 + 2 \cdot (a_2 - 0.5)^2 \cdot \left(1.145 - \frac{1}{\lambda_v}\right). \quad (17)$$

Similarly, Bey and Eigenberger[147] suggest the use of the correlation for solid cylinders with the inner void correction by Dixon,[181] while Foumeny and Benyahia[269] defined the interpenetration factor f^* with $f^* = f \cdot \left(1/a_2^2 - 1\right)$. This factor may take values ranging from 0.95-1.0, especially 0.97, depending on the aspect ratio a_2. In contrast, Benyahia and O'Neill[177] suggested a correlation suitable for all investigated aspect ratios:

$$\bar{\varepsilon} = \bar{\varepsilon}_{\text{inf}} + \frac{2.030}{(\lambda + 1.033)^2} \quad \text{with} \quad 1.9 \le \lambda_v \le 14.5$$
$$\bar{\varepsilon}_{\text{inf}} = 0.465. \quad (18)$$

Finally, investigations of the orientation distribution reveal that the majority of rings have their opening not facing in the main flow direction.[124]

In summary, a certain number of shapes, especially cylinders and hollow cylinders, have been investigated in the manner of packings of spheres. However, the existing data is not complete and differs significantly between the different sources consulted. While wall effect corrections have been derived for cylinders and hollow cylinders, the inclusion of the respective aspect ratios is inconsistent. Consequently, much more research is needed in order to understand the influence of simple shapes, such as cylinders and hollow cylinders alone, before thinking about more complex geometries.

2.4 | Influence of particle material

Although most researchers do not take any material effects into consideration, Schuster and Vortmeyer[122] realized a significant difference in the radial porosity profiles comparing glass and steel spheres of the same size. Susskind and Becker[211] compared steel and glass packings in random close packing arrangements, where the steel packing has a slightly higher overall porosity.

Regarding material diversity, packed shapes made of almost any imaginable material have been utilized. This includes glass,[20,67,119,120,122,125,129,175,179,180,190,191,193,211,270] ceramic,[119,124] steel,[122,186,193,211] stone,[196,217] metal,[182,192] lead,[103,105,106,108,111–113,217] wood,[121,231,240,241,247] beans[114,231] or other edibles,[114,232,243] and plastic[107,109,116,123,180,232] particles.

A small selection of studies evaluated packing material influences, but with contradictory results. While Crawford and Plumb[270] revealed a strong increase in packing porosity (from 0.356 to 0.442 and 0.467) with increasing surface roughness alias friction, while the in-depth material study performed by Macrae and Gray[225] resulted in only a minor influence of the coefficient of friction, if at all, but a significant impact of the coefficient of restitution where higher values decrease the packing porosity. Finally, Pottbäcker and Hinrichsen[186] observed both a decrease of porosity with lower friction and higher restitution values.

In summary, most researchers unjustifiably neglect the existing influence of material on the packing structure which may be problematic when comparing results with values taken from arbitrarily selected literature obtained under different conditions. However, the independent evaluation of the effect of material parameters remains impossible in experiments, as material parameters cannot be varied independently. Here, numerical tools are required to understand material-related features.

2.5 | Influence of tube shape and material

While almost all investigations employ cylindrical confinements, in some studies tubes with square cross-sections are used.[129,179] Comparing the average bed porosity data in a square duct[179] with those in a cylindrical duct,[135] very similar values are obtained. A range of studies relate to annular ring packings where the packing is interrupted in the bulk part by one or more introduced tubes.[102,108,111] These annular packings are typically applied in nuclear engineering. Furthermore, non-rigid containers (eg, balloons) were investigated by Susskind and Becker.[211] Additionally, Man et al[266] and Donev et al[271] used spherical containers in their studies; however, the difference between the results and those obtained for cylindrical containers was not discussed.

Besides the shape of the tube's cross-section, tubes having a wall structure comprised of hemispheres were investigated.[272–274] It was found that this adjustment may significantly flatten the porosity profile in the packings of spheres, especially close to the wall. Similarly, Foumeny et al[174,178] tried to improve the wall-section of a packing by introducing smaller particles into the wall region, forming a so-called stratified bed. In summary, the tube's shape and material are only seldomly discussed and evaluated probably as if they have only a minor effect on the overall packing conditions.

TABLE 7 Literature review on numerical packing generation studies sorted by shape

Source	Shape	Aspect ratio $1/a_1$	Aspect ratio a_x	$\bar{N}_c$	ϵ_{inf}	$\bar{\varepsilon}(\lambda)$	$\epsilon(r)$	θ
Wu et al[286]	Cube	1	-	✓	✓	✓	✓	-
Zhao et al[285]	Frustums, cylinder, cone	0.5-1.5	0-1	-	✓	-	-	-
Xie et al[344]	Cube	0.3-1.5	-	✓	✓	-	-	-
Zhao et al[345]	Spherocylinder	1-11	-	✓	✓	-	-	✓
Wouterse et al[346]	Spherocylinder	1-160	-	✓	✓	-	-	-
Wouterse et al[347]	Spherocylinder	1-6	-	✓	✓	-	-	-
Wouterse et al[347]	Ellipsoid	0.1-5	-	✓	✓	-	-	-
Donev et al[271]	Ellipsoid	0.3-3.5	-	✓	✓	-	-	-
Donev et al[271]	Aspherical ellipsoid	1-2	-	✓	✓	-	-	-
Williams and Philipse[348]	Spherocylinder	1-161	-	✓	✓	-	-	-
Sherwood[349]	Ellipsoids	0.07-15	-	-	✓	-	-	-
Various[46,90,108,112,139,161,276,297,298,300,304,309,320,332,350–355]	sphere	-	-	✓	✓	✓	✓	-
Qian et al[356]	Cylinder	0.1-10	-	✓	✓	-	-	-
Zhou et al[334]	Ellipsoid	0.1-7	-	✓	✓	✓	-	-
Zhao et al[357]	Superellipsoid	0.3-2.5	0.5-1.4	✓	✓	-	-	✓
Zhao et al[281]	Tetrahedra	0.4-3.0	−0.75-1.00	✓	✓	✓	-	✓
Zhao et al[358]	Sphero-tetrahedra	0.12-1.84	−0.75-1.000.05 to 10	-	✓	✓	-	-
Lathan et al[359]	Tetrahedra	1-1.8	-	-	✓	-	-	-
Li et al[360]	Tetrahedra	0.5-1.5	-	-	✓	-	-	-
Niegodajew and Marek[361]	Hollow cylinder	0.33-3.0	const. 0.8	-	✓	✓	-	✓
Nan et al[335]	Spherocylinder	5-20	-	✓	✓	-	-	-
Nan et al[362]	Spherocylinder	5-50	-	✓	✓	-	-	✓
Meng et al[207]	Spherocylinder	1-7	-	✓	✓	-	-	-
McGrother et al[363]	Spherocylinder	4-6	-	-	(✓)	-	-	-
Liu et al[364]	Cube	0.3-6.0	-	-	✓	-	-	-
Delaney and Cleary[333]	Superellipsoids	0.33-3.5	2-5	✓	✓	-	-	-
Li et al[289]	Cone	0.5-1.5	-	-	✓	-	-	-
	Cylinder	0.5-1.5	-	-	✓	-	-	-
	Ellipsoid	0.5-1	1-2	-	✓	-	-	-
	Spherocylinder	0.5-1.5	-	-	✓	-	-	-
	Tetrahedron	0.5-1.5	-	-	✓	-	-	-
Kyrylyuk and Philipse[365]	Spherocylinders	1-11	-	-	✓	-	-	-
Jiao and Torquato[366]	Platonic shapes	regular	-	-	✓	-	-	-
Jiao et al[367]	Superballs	regular	0-∞	✓	✓	-	-	-
Jia et al[293]	Cylinder	0.1-30	-	-	✓	-	-	-
	Spherocylinder	1-4.5	-	-	✓	-	-	-
Gan et al[368]	Ellipsoids	0.25-3.5	-	✓	✓	-	-	-
Evans and Ferrar[369]	Spherocylinder	1-25	-	-	✓	-	-	✓
Dong et al[319,370]	Cylinder	0.3-2.5	-	-	✓	-	-	-
	Ellipsoids	0.3-2.5	-	-	✓	✓	-	-

(Continues)

TABLE 7 (Continued)

Source	Shape	Aspect ratio $1/a_1$	Aspect ratio a_x	$\bar{N}_c$	ε_{inf}	$\bar{\varepsilon}(\lambda)$	$\epsilon(r)$	θ
Desmond and Franklin[371]	Ellipse	5-50	-	-	✓	-	-	-
Das et al[310]	Cube	0.33-1	-	-	✓	✓	✓	✓
Ferreiro-Cordova and Duijneveldt[372]	Spherocylinder	1-11	-	-	✓	-	-	-
Coelho et al[311]	Ellipsoid	0.1-10	-	-	✓	-	-	-
	Cylinder	0.1-10	-	-	✓	-	-	-
	Parallelepiped	0.1-10	-	-	✓	-	-	-
Chaikin et al[373]	Ellipsoid	1-3	0-1	✓	✓	-	-	-
Bolhuis and Frenkel[374]	Spherocylinder	1-4	-	-	(✓)	-	-	-
Blaak et al[375]	Cylinder	0.1-10	-	-	-	-	-	(✓)
Baule et al[376]	Lens	0.45-1	-	✓	✓	-	-	-
	Dimer	1-2	-	✓	✓	-	-	-
	Spherocylinder	1-2	-	✓	✓	-	-	-
Bargiel[377]	Spherocylinder	1-80	-	-	✓	-	-	-
Kyrylyuk et al[378]	Spherocylinder	1-4	-	-	✓	-	-	-
Abreu et al[379]	Spherocylinder	1-4.5	-	-	✓	-	-	-
Freeman et al[380]	Spherocylinder	5-35	-	-	✓	-	✓	-
Lumay and Vandewalle[219]	Cylinder	5-90	-	-	✓	-	-	-

3 | NUMERICALLY PACKED-BEDS

Numerical packing generation can be performed by a large selection of commercial or free software packages or an even larger selection of in-house produced codes and algorithms presented in the literature (see Bennett,[65] Clarke and Jónsson,[86] Jodrey and Tory,[88] Tory et al,[89] Visscher and Bolsterli,[275] Nolan and Kavanagh,[276] Yang et al,[277] and Zhong et al[26] and Zhu et al[278] for an overview). While the intention of this review is not to discuss advantages and disadvantages of each packing procedure, the DEM[279] is by now the most established tool for the numerical packing generation incorporating spheres with a physically accurate description of the particle packing process (see eg, Zhang et al[80] for details). Unfortunately, in order to pack particles other than spheres this method needs adaptation. For some distinct non-spherical shape classes, theoretical separate model developments exist (see Lu et al[280] for a general review, for more details also Zhao et al,[281] Kodam et al,[282,283] and Guo et al[284]). However, for the simulation of arbitrary shapes, it may be required to assemble the desired shape using a sufficiently large number of overlapping spheres.[248,283,285–291] Another attempt comprises the transfer of the DEM algorithm and the underlying physics to voxels (cubes) and the subsequent assembly of the desired shape by voxels.[112,292–295] Or, ignoring certain physical conditions, shapes can be represented by a surface grid.[296,297] A good comparison of some methods with regard to packing generation was presented by Fernengel et al[298] for spheres, Caulkin et al[291] for cylinders, and Flaischlen and Wehinger,[299] who investigated packings of cylinders, hollow cylinders, and some more complex shapes.

These numerical packing algorithms are frequently used to generate packings for subsequent fluid dynamics,[139,287,300–311] heat,[288,296,312–320] or mass transfer simulations.[321–331] The numerical procedures are well capable of geometric packing analysis, allowing separate material property variation, packing procedure evaluation, and shape factor analysis on a large scale and in a fast and cost-efficient manner. In general, two settings have to be distinguished, one setting incorporating the confining wall (see Zhao et al,[281] and Mueller[332]) and one setting having periodic boundaries and thus neglecting of the influence of the confining wall (see Zhao et al,[285] and Delaney and Cleary[333]). When using confined packings, it is required to use the bulk part of the packing for porosity calculation to exclude top and bottom effects.[232] Unfortunately, validation is frequently a major problem, as typically not enough experimental data is available, and the

available data frequently has a large error or is obtained under uncertain or vague packing and material conditions.

3.1 | Influence of material and packing procedure

Zhang et al[80] evaluated packing procedure properties and found a decrease in porosity when using higher particle drop heights and lower deposition intensities (number of particles filled per second). Additionally, material properties have been evaluated predicting a lower porosity when having a lower damping coefficient which directly correlates to the coefficient of restitution and a lower coefficient of friction.[80] Similar results were obtained by other scientists.[248] The decrease in porosity for a smaller coefficient of friction values was repeatedly obtained.[140,161,290,297,334–337] Furthermore, the porosity increases with increasing E-modulus,[248,334] a decrease in the coefficient of restitution,[297,335,336] and an increase in surface energy.[335] The porosity is not dependent on the particle's stiffness.[335] The extent to which it is influenced by certain material parameters can be best evaluated using a sensitivity analysis.[338] However, the respective material parameters are often not known, they need to be guessed and adjusted by comparing experimental and numerical outputs.[339]

Packing densification using vibration,[213,286,340] tapping,[341,342] or air impact densification[343] was studied finding optimal densification parameters to gain the

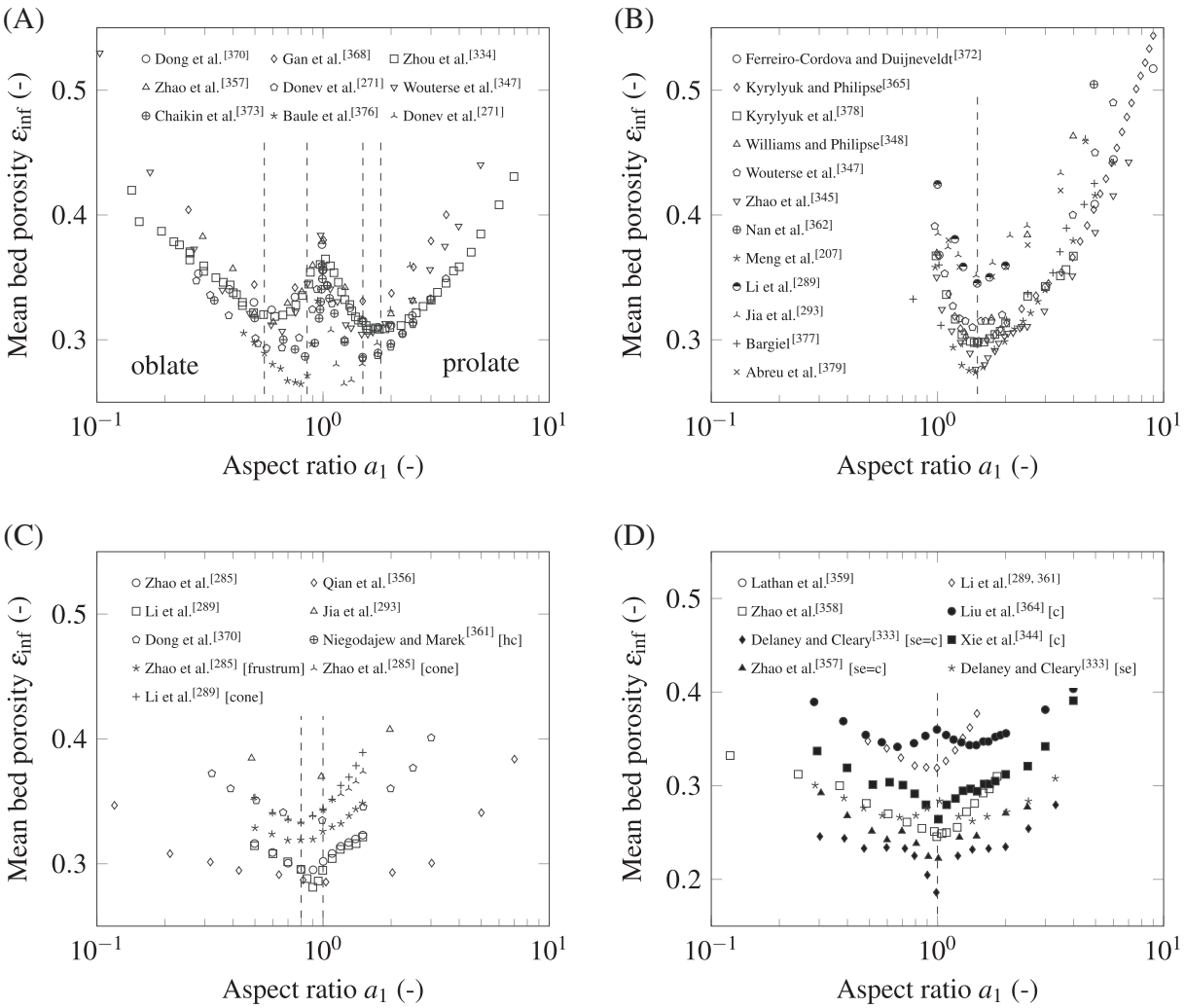

FIGURE 12 Mean bed porosity under the absence of confinement as a function of the aspect ratio of packings consisting of: A, ellipsoids, aspherical ellipses (Donev et al[271]) and lenses (Baule et al[376]); B, spherocylinders; C, cylinders (empty marks), hollow cylinders [hc], frustums and cones; and D, tetrahedra (empty marks), cubes (solid marks) and superellipsoids (star). The vertical line marks the range of minima occurrence[207,271,285,289,293,333,334,344,345,347,348,356–362,364,365,368,370,372,373,376–379]

densest packings. Furthermore, a lower porosity can be obtained with fewer particles added at the same time.[80,298,336] Thus, numerical packing generation tools are very important for the evaluation of material or packing procedure parameters and thus understanding of these influences, because it is impossible to vary these independently in an experiment.

3.2 | Influence of the shape

Numerical studies investigating shape effects on packing structure, most predominantly aspect ratio variations, are reviewed in Table 7, clustered according to the evaluated shapes and respective aspect ratio ranges, and the evaluated packing parameters including mean coordination number $\bar{N}_C$, bulk porosity ε_{inf} and $\bar{\varepsilon}(\lambda)$, local porosity distribution $\varepsilon(r)$, and the particle orientation angle θ. Additionally, the data obtained from the literature for the calculated average bed porosity as a function of the respective aspect ratio are summarized in Figure 12, especially regarding: (a) ellipsoid shapes, (b) spherocylinders, (c) cylindrical shapes, and (d) platonic shapes. In some cases, correlations for calculating the porosity based on the respective aspect ratios are suggested.[285] The influence of curl index when packing curved spherocylinders was studied,[362] along with the influence of particle orientation.[361,362] For instance, in a packing of hollow cylinders, the particle orientation is increasingly perpendicular to the container axis with increasing aspect ratio a_1.[361]

Comparing different geometries,[289,381] a shape packing density order was identified. Accordingly, the lowest porosity values were obtained with cubes followed by ellipsoids, cylinders and spherocylinders, tetrahedrons, cones, and finally spheres with the highest bulk porosity.[289] As shown in Figure 12, the aspect ratios with the lowest packing porosity were identified to be around unity, except for the spherocylinders and ellipsoids, where the minima are around 1.35 and 0.7.

Despite the usage of rather mathematical shapes, Partopour and Dixon[296] compared packings of actual catalyst shapes such as hollow cylinders and multi-holed/fluted versions. Similarly, Moghaddam et al[336] compared sphere, cylinder, and hollow cylinder packings in cylindrical confining walls, especially regarding the radial porosity distribution and λ-relation. Khartik and Buwa[328] compared single-pellet-string packings of six different pellet shapes used in catalysis, comprising multi-holed cylinders, cross-web cylinders, and poly-lobes, and Caulkin et al[111,124] investigated packings of cylinders with different hole geometries and reactor setups. Finally, trilobes were further studied by Boccardo et al.[297]

In summary, numerical packing generation tools have been frequently used to evaluate particle aspect ratio variations affecting the bulk porosity. However, as the range of imaginable shapes and their aspect ratio variations are infinite, we are far away from understanding a general shape influence on packed beds. Moreover, comparing the obtained results, large deviations can be seen relating to different material and packing mode conditions. Consequently, before being able to evaluate a universal shape dependence, the definition of standard packing conditions is required. Otherwise, results are impossible to compare.

3.3 | Further notable results

Besides the often studied shape, material, and packing mode variations, some further notable studies were performed, for instance comprising confinement shape variations including cylindrical, half-cylindrical, square, and rectangular cross-sections.[307,319] Moreover, studies were performed addressing the porosity increase and packing compression for packing particle sizes <1000 μm where interparticle forces become relevant.[1,368,382,383] Further studies address the effect of particle size distribution or bi-, tri-, and multi-modal particle mixtures of the same shape or of different shapes (see Caulkin et al,[112] Kyrylyuk et al,[378] and Dorai et al[384]), but his is outside the scope of this review.

4 | CONCLUSION

The knowledge of random packings of mono-sized particles gained over the last hundred years of research was reviewed and clustered. Available studies regarding the influence of shape, size, and material properties of the particles, the packing and densification mode characterizing the bed formation, and the influence of the confining tube including tube shape and material, were taken into consideration. Explicitly excluded is the influence of shape inhomogeneity and multi-modal or multi-shape particle mixtures. Furthermore, the reviewed data is restricted to a minimum particle size of 1 mm where gravity is the predominant force. The structural characteristics investigated comprise the mean coordination number, the radial and axial porosity distributions, and the average bed porosity. While a significant amount of complementary studies with regard to packed-beds of spheres are known to result in a good understanding of structural bed characteristics, there is still a significant lack of knowledge with regard to the influence of particle shape. While this cannot be attributed to a lack of data, as there are numerous studies addressing shape influences on all levels, the research field is simply too large for these studies to lead to a complete

fundamental understanding. However, numerical tools capable of producing and evaluating huge data sets in short time frames open up the possibility to take the research on packing characteristics to another level, and the overall complexity will rise when transferring to the real applications of packed-beds. Structural impacts on fluid dynamics, heat, and mass transfer are far away from being comprehensively understood while trial and error remain the standard development method. Consequently, the development of packing shapes might be an interesting application example where machine learning tools might become relevant in the future.

ACKNOWLEDGEMENTS

Financial and substantial support of MuniCat, a strategic alliance between the Technical University of Munich (TUM) and Clariant AG is gratefully acknowledged. J.v.S. would further like to thank the TUM Graduate School for their generous support. Open access funding enabled and organized by Projekt DEAL. WOA Institution: Technische Universitat Munchen Blended DEAL: ProjektDEAL.

CONFLICT OF INTEREST

The authors declare no potential conflict of interests.

AUTHOR CONTRIBUTIONS

The research "Review on the Structure of Random Packed-Beds" was initiated by Jennie von Seckendorff and supervised by Olaf Hinrichsen. The review was written by Jennie von Seckendorff and supported by Olaf Hinrichsen.

NOMENCLATURE

Latin symbols

a,b,c,d	pre-factor parameters (−)
a_1	height to diameter aspect ratio (−)
a_2	inner to outer diameter aspect ratio (−)
a_3	upper to lower diameter aspect ratio (−)
a_p	particle surface area (m^2)
a_x	any other aspect ratio (−)
$c_D(Re)$	drag coefficient (−)
d	real particle diameter (m)
d_i	inner particle diameter of hollow cylinder (m)
d_p	particle diameter (m)
d_{ps},d_{pv}, d_{pw}, d_{pd},d_{pack}	equivalent particle diameter (m)
D	diameter of tube (m)
f	hollow cylinder interpenetration correction (−)
F_D	drag force (N)
g	acceleration of gravity ($\frac{m}{s^2}$)
h	real height of a particle (m)
H	height of tube (m)
H_r	Hausner ratio (−)
m	flatness ratio (−)
n	number of taps per second (s^{-1})
n	elongation ratio (−)
$\bar{N}_c$	mean contact number (−)
r	radial position (m)
R	tube radius (m)
u_0	superficial velocity ($\frac{m}{s}$)
u_s	sedimentation velocity ($\frac{m}{s}$)
T	tortuosity (−)
v_p	particle volume (m^3)
z	axial position (m)
z_{min}	radial location of first porosity minimum (−)
z_r	non-dimensional radial position (−)
z_z	non-dimensional axial position (−)

Greek symbols

ε	porosity (−)
$\bar{\varepsilon}$	average bed porosity (−)
ε_{inf}	average bed porosity with $\lambda \to \infty$ (−)
ε_{min}	local porosity at the first minimum close to the tube wall (−)
$\bar{\varepsilon}_{sc}$	average reference porosity of a solid cylinder (−)
$\varepsilon(r)$	radial porosity distribution (−)
$\varepsilon(z)$	axial porosity distribution (−)
$\bar{\varepsilon}(\lambda)$	average porosity as a function of λ (−)
λ	tube to particle diameter ratio (−)
λ_v	tube to particle diameter ratio based on volume equivalent particle diameter (−)
$\bar{\varrho}_\epsilon$	packing density, $=1-\bar{\varepsilon}$ (−)
ϱ_f	fluid density ($\frac{kg}{m^3}$)
ϱ_p	particle density ($\frac{kg}{m^3}$)
τ	relaxation time (s^{-1})
κ	tube height-to-particle diameter ratio (−)
Ψ_W	sphericity (−)
ψ	azimuthal contact angle (°)
θ	particle orientation in packing (°)
$\bar{\phi}_c$	mean (poloidal) contact angle (°)

PEER REVIEW

The peer review history for this article is available at https://publons.com/publon/10.1002/cjce.23959

REFERENCES

[1] M. Dorn, F. Eschbach, D. Hekmat, D. Weuster-Botz, *J. Chromatogr. A* **2017**, *1516*, 89.

[2] K. K. Unger, R. Skudas, M. M. Schulte, *J. Chromatogr. A* **2008**, *1184*, 393.
[3] G. Guiochon, T. Farkas, H. Guan-Sajonz, J. H. Koh, M. Sarker, B. J. Stanley, T. Yun, *J. Chromatogr. A* **1997**, *762*, 83.
[4] F. S. Mederos, J. Ancheyta, J. Chen, *Appl. Catal. A* **2009**, *355*, 1.
[5] G. Eigenberger, in *Handbook of Heterogeneous Catalysis*, 2nd ed. (Eds: C. Ertl, H. Knözinger, F. Schüth, J. Weitkamp), Wiley-VCH, Weinheim, Germany **2008**.
[6] M. Baerns, A. Behr, A. Brehm, J. Gmehling, H. Hofmann, U. Onken, A. Renken, *Technische Chemie*, 2nd ed., Wiley-VCH, Weinheim, Germany **2014**.
[7] A. Mersmann, M. Kind, J. Stichlmair, *Thermal Separation Technology: Principles, Methods, Process Design*, 1st ed., Springer-Verlag, Berlin, Heidelberg, Germany **2011**.
[8] A. Koster, H. D. Matzner, D. R. Nicholsi, *Nucl. Eng. Des.* **2003**, *222*, 231.
[9] S. Thomas, *Energy Policy* **2011**, *39*, 2431.
[10] G. J. Auwerda, J. L. Kloosterman, A. J. M. Winkelman, J. Groen, V. Dijk, presented at Advances in Reactor Physics to Power the Nuclear Renaissance, Pittsburgh, PA, May 2010.
[11] G. Jacob, C. U. Brown, A. Donmez, *The Influence of Spreading Metal Powders with Different Particle Size Distributions on the Powder Bed Density in Laser-based Powder Bed Fusion Processes*, NIST Advanced Manufacturing Series, National Institute of Standards and Technology, Gaithersburg, MD **2018**.
[12] H. Singh, R. P. Saini, J. S. Saini, *Renewable Sustainable Energy Rev.* **2010**, *14*, 1059.
[13] C. D. F. Rogers, T. A. Dijkstra, I. J. Smalley, *Earth-Sci. Rev.* **1994**, *36*, 59.
[14] S. W. Taylor, P. C. D. Milly, P. R. Jaffré, *Water Resour. Res.* **1990**, *26*, 2161.
[15] A. J. Cooke, R. K. Rowe, *J. Environ. Eng.* **1999**, *125*, 126.
[16] A. I. Rodarte-Morales, G. Feijoo, M. T. Moreira, J. M. Lema, *Biochem. Eng. J.* **2012**, *66*, 38.
[17] M. Horttanainen, J. Saastamoinen, P. Sarkomaa, *Energy Fuels* **2002**, *16*, 676.
[18] E. López, E. Heracleous, A. A. Lemonidou, D. O. Borio, *Chem. Eng. J.* **2008**, *145*, 308.
[19] A. Klyushina, K. Pacultová, L. Obalová, *React. Kinet. Mech. Catal.* **2015**, *115*, 651.
[20] A. De Klerk, *AIChE J.* **2003**, *49*, 2022.
[21] D. P. Haughey, G. S. G. Beveridge, *Can. J. Chem. Eng.* **1969**, *47*, 130.
[22] B. Eisfeld, K. Schnitzlein, *Chem. Eng. Sci.* **2005**, *60*, 4105.
[23] E. Erdim, Ö. Akgiray, I. Demir, *Powder Technol.* **2015**, *283*, 488.
[24] J. M. P. Q. Delgado, *Heat Mass Transfer* **2006**, *42*, 279.
[25] W. Antwerpen, C. G. Du Toit, P. G. Rousseau, *Nucl. Eng. Des.* **2010**, *240*, 1803.
[26] W. Zhong, A. Yu, X. Liu, Z. Tong, H. Zhang, *Powder Technol.* **2016**, *302*, 108.
[27] W.-C. Yang, *Handbook of Fluidization and Fluid-Particle Systems*, 1st ed., CRC Press, Boca Raton, FL **2003**.
[28] S. Afandizadeh, E. A. Foumeny, *Appl. Therm. Eng.* **2001**, *21*, 669.
[29] Y. Tsutsumi, *Powder Technol.* **1973**, *7*, 181.
[30] E. Manegold, R. Hofmann, K. Solf, *Kolloid-Z.* **1931**, *56*, 142.
[31] L. C. Graton, H. J. Fraser, *J. Geol.* **1935**, *43*, 785.
[32] J. Hrubíšek, *Kolloid-Beih.* **1941**, *53*, 385.
[33] J. Kubie, *Chem. Eng. Sci.* **1988**, *43*, 1403.
[34] J. D. Bernal, *Proc. R. Soc. A* **1964**, *280*, 299.
[35] D. Kunii, J. M. Smith, *AIChE J.* **1960**, *6*, 71.
[36] J. S. Goodling, M. S. Khader, *Powder Technol.* **1985**, *44*, 53.
[37] W. O. Smith, P. D. Foote, P. F. Busang, *Phys. Rev.* **1929**, *34*, 1271.
[38] J. D. Bernal, J. Mason, *Nature* **1960**, *188*, 910.
[39] J. Wadsworth, *Experimental Examination of Local Processes in Packed Beds of Homogeneous Spheres*, National Research Council of Canada, Ottawa, Canada **1960**.
[40] M. Arakawa, M. Nishino, *J. Soc. Mater. Sci. Jpn.* **1973**, *22*, 658.
[41] D. Pinson, R. P. Zou, A. B. Yu, P. Zulli, M. J. McCarthy, *J. Phys. D: Appl. Phys.* **1998**, *31*, 457.
[42] M. Oda, *Soils Found.* **1977**, *17*, 29.
[43] G. D. Scott, *Nature* **1960**, *188*, 908.
[44] T. Aste, M. Saadatfar, A. Sakellariou, T. J. Senden, *Phys. A* **2004**, *339*, 16.
[45] T. Aste, M. Saadatfar, T. J. Senden, *Phys. Rev. E* **2005**, *71*, 061302.
[46] G. J. Auwerda, J.-L. Kloosterman, D. Lathouwers, T. H. J. J. Hagen, *Nucl. Technol.* **2013**, *183*, 272.
[47] R. P. Zou, X. Bian, D. Pinson, R. Y. Yang, A. B. Yu, P. Zulli, *Part. Part. Syst. Charact.* **2003**, *20*, 335.
[48] G. A. Georgalli, M. A. Reuter, *Miner. Eng.* **2006**, *19*, 246.
[49] J. Reimann, J. Vicente, E. Brun, C. Ferrero, Y. Gan, A. Rack, *Powder Technol.* **2017**, *318*, 471.
[50] J. Reimann, R. A. Pieritz, C. Ferrero, M. Michiel, R. Rolli, *Fusion Eng. Des.* **2008**, *83*, 1326.
[51] J. Reimann, R. A. Pieritz, R. Rolli, *Fusion Eng. Des.* **2006**, *81*, 653.
[52] G. D. Scott, *Nature* **1962**, *194*, 956.
[53] G. Mason, W. Clark, *Nature* **1965**, *207*, 512.
[54] G. Mason, W. Clark, *Nature* **1966**, *211*, 957.
[55] G. D. Scott, D. L. Mader, *Nature* **1964**, *201*, 382.
[56] J. L. Finney, *Proc. R. Soc. London Ser. A* **1970**, *319*, 479.
[57] J. Urquidi, S. Singh, C. H. Cho, G. W. Robinson, *Phys. Rev. Lett.* **1999**, *83*, 2348.
[58] A. O. Dohn, E. Biasin, K. Haldrup, M. M. Nielsen, N. E. Henriksen, K. B. Moller, *J. Phys. B: At. Mol. Opt. Phys.* **2015**, *48*, 244010.
[59] A. K. Soper, *ISRN Phys. Chem.* **2013**, *11*, 279463.
[60] H. P. Meissner, A. S. Michaels, R. Kaiser, *Ind. Eng. Chem. Process Des. Dev.* **1964**, *3*, 202.
[61] S. Melmore, *Nature* **1942**, *149*, 412.
[62] H. Heesch, F. Laves, *Z. Kristallogr. - Cryst. Mater.* **1933**, *85*, 443.
[63] M. Nakagaki, H. Sunada, *Yakugaku Zasshi* **1968**, *88*, 651.
[64] M. Suzuki, T. Oshima, *KONA Powder Part. J.* **1989**, *7*, 22.
[65] C. H. Bennett, *J. Appl. Phys.* **1972**, *43*, 2727.
[66] A. B. Yu, J. Bridgwater, A. Burbidge, *Powder Technol.* **1997**, *92*, 185.
[67] C. L. Feng, A. B. Yu, *Powder Technol.* **1998**, *99*, 22.
[68] J. V. Milewski, *Handbook of Fillers and Reinforcements for Plastics*, 1st ed., Van Nostrand Reinhold, New York **1987**.
[69] M. Suzuki, H. Sato, M. Hasegawa, M. Hirota, *Powder Technol.* **2001**, *118*, 53.
[70] R. Y. Yang, R. P. Zou, A. B. Yu, *Phys. Rev. E* **2000**, *62*, 3900.
[71] J. X. Liu, T. J. Davies, *Powder Metall.* **1997**, *40*, 48.
[72] J. M. Beck, V. A. Volpert, *J. Colloid Interface Sci.* **2003**, *262*, 162.
[73] M. E. Wise, *Philips Res. Rep.* **1952**, *7*, 321.
[74] M. J. Hogendijk, *Philips Res. Rep.* **1963**, *18*, 109.

[75] J. A. Dodds, *J. Colloid Interface Sci.* **1980**, *77*, 317.
[76] M. Leitzelement, C. S. Lo, J. Dodds, *Powder Technol.* **1985**, *41*, 159.
[77] P. Richard, L. Oger, J. P. Troadec, A. Gervois, *Eur. Phys. J. E: Soft Matter Biol. Phys.* **2001**, *6*, 295.
[78] A. B. Yu, N. Standish, *Powder Technol.* **1988**, *55*, 171.
[79] H. Iwata, T. Homma, *Powder Technol.* **1974**, *10*, 79.
[80] Z. P. Zhang, L. F. Liu, Y. D. Yuan, A. B. Yu, *Powder Technol.* **2001**, *116*, 23.
[81] M. Suzuki, T. Oshima, *Powder Technol.* **1985**, *44*, 213.
[82] M. Suzuki, T. Oshima, *Powder Technol.* **1983**, *35*, 159.
[83] M. Suzuki, K. Makino, M. Yamada, K. Linoya, *Kagaku Kogaku Ronbunshu* **1980**, *6*, 59 (in Japanese).
[84] L. Oger, J. P. Troadec, D. Bideau, J. A. Dodds, M. J. Powell, *Powder Technol.* **1986**, *46*, 121.
[85] L. Y. Yi, K. J. Dong, R. P. Zou, A. B. Yu, *Ind. Eng. Chem. Res.* **2011**, *2011*, 8773.
[86] A. S. Clarke, H. Jónsson, *Phys. Rev. E* **1993**, *47*, 3975.
[87] L. Meng, P. Lu, S. Li, *Particuology* **2014**, *16*, 155.
[88] W. S. Jodrey, E. M. Tory, *Phys. Rev. A* **1985**, *32*, 2347.
[89] E. M. Tory, B. H. Church, M. K. Ratner, A. D. N. M. Tam, *Can. J. Chem. Eng.* **1973**, *51*, 484.
[90] X. Z. An, K. J. Dong, R. Y. Yang, R. P. Zou, C. C. Wang, A. B. Yu, *Granular Matter* **2016**, *18*, 1.
[91] C. G. Du Toit, W. Antwerpen, P. G. Rousseau, presented at ICAPP Conf. 2009, Tokyo, Japan, May 2009.
[92] H. Rumpf, *Chem. Ing. Tech.* **1958**, *30*, 144.
[93] W. G. Field, in *Proceedings of the 4th Australian and New Zealand Conf. on Soil Mechanics*, Institution of Engineers, Sydney **1963**, p. 143.
[94] D. P. Haughey, G. S. G. Beveridge, *Chem. Eng. Sci.* **1966**, *21*, 905.
[95] K. Ridgway, K. J. Tarbuck, *Br. Chem. Eng.* **1967**, *12*, 384.
[96] N. W. Ridgway, G. A. Tingate, *Aust. A. E. C.* **1970**, *E202*, 16.
[97] K. Gotoh, *J. Soc. Powder Technol. Jpn.* **1978**, *15*, 220 (in Japanese).
[98] T. Nagao, *Jpn. Soc. Mech. Eng.* **1978**, *44*, 1912.
[99] N. Ouchiyama, T. Tanaka, *Ind. Eng. Chem. Fundam.* **1980**, *19*, 338.
[100] M. Suzuki, K. Makino, M. Yamada, K. Linoya, *Int. Chem. Eng.* **1981**, *21*, 482.
[101] D. He, N. N. Ekere, L. Cai, *Phys. Rev. E* **1999**, *60*, 7098.
[102] F. A. Schneider, D. W. T. Rippin, *Ind. Eng. Chem. Res.* **1988**, *27*, 1936.
[103] S. Roshani, *PhD thesis*, University of Leeds, Leeds, UK **1990**.
[104] L. H. S. Roblee, R. M. Baird, J. W. Tierney, *AIChE J.* **1958**, *4*, 460.
[105] R. F. Benenati, C. B. Brosilow, *AIChE J.* **1962**, *8*, 359.
[106] M. Propster, J. Szekely, *Powder Technol.* **1977**, *17*, 123.
[107] J. S. Goodling, R. I. Vachon, W. S. Stelpflug, S. J. Ying, M. S. Khader, *Powder Technol.* **1983**, *35*, 23.
[108] C. G. Du Toit, *Nucl. Eng. Des.* **2008**, *238*, 3073.
[109] M. C. Thadani, F. N. Peebles, *Ind. Eng. Chem. Process Des. Dev.* **1966**, *5*, 265.
[110] R. Küfner, H. Hofmann, *Chem. Eng. Sci.* **1990**, *45*, 2141.
[111] R. Caulkin, A. Ahmad, M. Fairweather, X. Jia, R. A. Williams, *Comput. Chem. Eng.* **2009**, *33*, 10.
[112] R. Caulkin, M. Fairweather, X. Jia, N. Gopinathan, R. A. Williams, *Comput. Chem. Eng.* **2006**, *30*, 1178.
[113] J. H. Ismail, M. Fairweather, K. H. Javed, *Chem. Eng. Res. Des.* **2002**, *80*, 645.
[114] W. Du, N. Quan, P. Lu, J. Xu, W. Wei, L. Zhang, *Chem. Eng. Res. Des.* **2016**, *106*, 115.
[115] A. Montillet, L. Coq, *Powder Technol.* **2001**, *121*, 138.
[116] K. Ridgway, K. J. Tarbuck, *J. Pharm. Pharmacol.* **1966**, *18*, 168S.
[117] M. R. Shaffer, *Master's thesis*, Purdue University, Lafayette, IN **1953**.
[118] N. B. Griffiths, *PhD thesis*, University of Cambridge, Cambridge **1986**.
[119] J. J. Lerou, G. F. Froment, in *Chemical Reactor Design and Technology*, NATO ASI Series (Ed: H. I. Lasa), Springer, Dordrecht, The Netherlands **1986**, p. 729.
[120] V. Staněk, V. Eckert, *Chem. Eng. Sci.* **1979**, *34*, 933.
[121] K. K. Pillai, *Chem. Eng. Sci.* **1977**, *32*, 59.
[122] J. Schuster, D. Vortmeyer, *Chem. Ing. Tech.* **1980**, *52*, 848.
[123] V. N. Korolev, N. I. Syromyatnikov, E. M. Tolmachev, *J. Eng. Phys.* **1971**, *21*, 1475.
[124] R. Caulkin, X. Jia, C. Xu, M. Fairweather, R. A. Williams, H. Stitt, M. Nijemeisland, S. Aferka, M. Crine, A. Léonard, D. Toye, P. Marchot, *Ind. Eng. Chem. Res.* **2009**, *48*, 202.
[125] F. Al-Falahi, M. Al-Dahhan, *Nucl. Eng. Des.* **2016**, *310*, 231.
[126] R. A. Pieritz, J. Reimann, C. Ferrero, *Adv. Eng. Mater.* **2010**, *13*, 145.
[127] N. J. Mariani, W. I. Salvat, M. A. Campesi, G. F. Barreto, O. M. Martínez, *Int. J. Chem. React. Eng.* **2009**, *7*, A82.
[128] X. Gan, M. Kamlah, J. Reimann, *Fusion Eng. Des.* **2010**, *85*, 1782.
[129] J. M. Buchlin, M. Riethmuller, J. J. Ginoux, *Chem. Eng. Sci.* **1977**, *32*, 1116.
[130] R. Balzan, A. L. Sellerio, D. Mari, A. Comment, G. Gremaud, *Granular Matter* **2013**, *15*, 873.
[131] R. Balzan, A. L. Sellerio, D. Mari, A. Comment, *Appl. Magn. Reson.* **2015**, *46*, 633.
[132] R. Stannarius, *Rev. Sci. Instrum.* **2017**, *88*, 051806.
[133] A. J. Sederman, P. Alexander, L. F. Gladden, *Powder Technol.* **2001**, *117*, 255.
[134] N. L. Nguyen, V. Buren, R. Reimert, A. Garnier, *Magn. Reson. Imaging* **2005**, *23*, 395.
[135] G. E. Mueller, *Powder Technol.* **1992**, *72*, 269.
[136] M. Giese, K. Rottschäfer, D. Vortmeyer, *AIChE J.* **1998**, *44*, 484.
[137] K. Ridgway, K. J. Tarbuck, *Chem. Eng. Sci.* **1968**, *23*, 1147.
[138] M. Suzuki, T. Shinmura, K. Iimura, M. Hirota, *Adv. Powder Technol.* **2008**, *19*, 183.
[139] P. Lovreglio, S. Das, K. A. Buist, E. A. J. F. Peters, L. Pel, J. A. M. Kuipers, *AIChE J.* **2018**, *64*, 1896.
[140] C. M. Wensrich, *Powder Technol.* **2012**, *219*, 118.
[141] C. E. Schwartz, J. M. Smith, *Ind. Eng. Chem.* **1953**, *45*, 1209.
[142] G. Johnson, *PhD thesis*, University of Rochester, Rochester, NY **1970**.
[143] H. A. Moallemi, *PhD thesis*, University of Leeds, Leeds, UK **1989**.
[144] B. C. Chandrasekhara, D. Vortmeyer, *Wärme- und Stoffübertragung* **1979**, *12*, 105.
[145] H. Martin, *Chem. Eng. Sci.* **1978**, *33*, 913.
[146] Y. Cohen, A. B. Metzner, *AIChE J.* **1981**, *27*, 705.
[147] O. Bey, G. Eigenberger, *Chem. Eng. Sci.* **1997**, *52*, 1365.
[148] M. Giese, *PhD thesis*, Technische Universität München, Munich, Germany **1998**.
[149] D. Vortmeyer, J. Schuster, *Chem. Eng. Sci.* **1983**, *38*, 1691.
[150] P. Cheng, C. T. Hsu, *Int. J. Heat Mass Transfer* **1986**, *29*, 1843.

[151] J. R. Sodré, J. A. R. Parise, *Exp. Therm. Fluid Sci.* **1998**, *17*, 265.
[152] M. L. Hunt, C. L. Tien, *Chem. Eng. Sci.* **1990**, *45*, 55.
[153] G. E. Mueller, *Powder Technol.* **2019**, *342*, 607.
[154] G. E. Mueller, *Chem. Eng. Sci.* **1991**, *46*, 706.
[155] G. E. Mueller, *Powder Technol.* **2010**, *203*, 626.
[156] V. M. H. Govindarao, G. F. Froment, *Chem. Eng. Sci.* **1986**, *41*, 533.
[157] V. M. H. Govindarao, K. V. S. Ramrao, *Chem. Eng. Sci.* **1988**, *43*, 2544.
[158] V. M. H. Govindarao, M. Subbanna, A. V. S. Rao, K. V. S. Ramrao, *Chem. Eng. Sci.* **1990**, *45*, 362.
[159] N. J. Mariani, W. I. Salvat, O. M. Martínez, G. F. Barreto, *Can. J. Chem. Eng.* **2002**, *80*, 186.
[160] V. M. H. Govindarao, K. V. S. Ramrao, A. V. S. Rao, *Chem. Eng. Sci.* **1992**, *47*, 2105.
[161] J. Theuerkauf, P. Witt, D. Schwesig, *Powder Technol.* **2006**, *165*, 92.
[162] C. G. Du Toit, *Powder Technol.* **2019**, *342*, 475.
[163] F. Lamarche, C. Leroy, *Comput. Phys. Commun.* **1990**, *59*, 359.
[164] N. J. Mariani, O. M. Martínez, G. F. Barreto, *Chem. Eng. Sci.* **2001**, *56*, 5693.
[165] N. J. Mariani, G. D. Mazza, O. M. Martínez, G. F. Barreto, *Can. J. Chem. Eng.* **2000**, *78*, 1133.
[166] G. E. Mueller, *Powder Technol.* **2012**, *229*, 90.
[167] M. Alonso, M. Satoh, K. Miyanami, *Can. J. Chem. Eng.* **1992**, *70*, 28.
[168] K. Shinohara, T. Murai, *J. Ceram. Soc. Jpn.* **1993**, *101*, 1369.
[169] M. Alonso, E. Sainz, F. A. Lopez, K. Shinohara, *Chem. Eng. Sci.* **1995**, *50*, 1983.
[170] K. Gotoh, M. Nakagawa, M. Furuuchi, A. Yoshigi, *J. Chem. Phys.* **1986**, *85*, 3078.
[171] J. L. Finney, J. Wallace, *J. Non-Cryst. Solids* **1981**, *43*, 165.
[172] H. J. Frost, *Acta Metall.* **1982**, *30*, 889.
[173] S. Prager, *Chem. Eng. Sci.* **1963**, *18*, 227.
[174] E. A. Foumeny, H. A. Moallemi, C. Mcgreavy, J. A. A. Castro, *Can. J. Chem. Eng.* **1991**, *69*, 1010.
[175] R. P. Zou, A. B. Yu, *Chem. Eng. Sci.* **1995**, *50*, 1504.
[176] C. G. Du Toit, *Nucl. Eng. Des.* **2020**, *359*, 110451.
[177] F. Benyahia, K. E. O'Neill, *Part. Sci. Technol.* **2005**, *23*, 169.
[178] E. A. Foumeny, S. Roshani, *Chem. Eng. Sci.* **1991**, *46*, 2363.
[179] G. S. Beavers, E. M. Sparrow, D. E. Rodenz, *J. Appl. Mech.* **1973**, *40*, 655.
[180] E. A. Foumeny, A. Kulkarni, S. Roshani, A. Vatani, *Appl. Therm. Eng.* **1996**, *16*, 195.
[181] A. G. Dixon, *Can. J. Chem. Eng.* **1988**, *66*, 705.
[182] J. E. Ayer, F. E. Soppet, *J. Am. Ceram. Soc.* **1965**, *48*, 180.
[183] R. Jeschar, *Arch. Eisenhüttenwes.* **1964**, *35*, 91.
[184] A. M. Ribeiro, P. Neto, C. Pinho, *Int. Rev. Chem. Eng.* **2010**, *2*, 40.
[185] G. Sonntag, *Chem. Ing. Tech.* **1960**, *32*, 317.
[186] J. Pottbäcker, O. Hinrichsen, *Chem. Ing. Tech.* **2017**, *89*, 454.
[187] M. Leva, M. Grummer, *Chem. Eng. Prog.* **1947**, *43*, 713.
[188] C. McGreavy, E. A. Foumeny, K. H. Javed, *Chem. Eng. Sci.* **1986**, *41*, 787.
[189] T. C. S. Hsiang, H. W. Haynes, *Chem. Eng. Sci.* **1977**, *32*, 678.
[190] C. F. Chu, K. M. Ng, *AIChE J.* **1989**, *35*, 148.
[191] R. M. Fand, R. Thinakaran, *J. Fluids Eng.* **1990**, *112*, 84.
[192] R. K. McGeary, *J. Am. Ceram. Soc.* **1961**, *44*, 513.
[193] R. C. Raichura, *Exp. Heat Transfer* **1999**, *12*, 309.
[194] A. Montillet, E. Akkari, J. Comiti, *Chem. Eng. Process.* **2007**, *46*, 329.
[195] R. M. Fand, M. Sundaram, M. Varahasamy, *J. Fluids Eng.* **1993**, *115*, 169.
[196] W. Reichelt, *Chem. Ing. Tech.* **1972**, *44*, 1068.
[197] M. Leva, *Chem. Eng.* **1949**, *55*, 115.
[198] D. E. Beasley, J. A. Clark, *Int. J. Heat Mass Transfer* **1984**, *27*, 1659.
[199] Z. Guo, Z. Sun, N. Zhang, M. Ding, J. Wen, *Chem. Eng. Sci.* **2017**, *173*, 578.
[200] Z. Guo, Z. Sun, N. Zhang, X. Cao, M. Ding, *Powder Technol.* **2019**, *354*, 842.
[201] P. Carman, *Trans. Inst. Chem. Eng.* **1937**, *15*, 150.
[202] M. E. Aerov, *PhD thesis*, Moscow University **1951**.
[203] G. F. Froment, K. B. Bischoff, *Chemical Reactor Analysis and Design*, 2nd ed., Wiley, New York **1979**.
[204] A. S. Puschnov, *Khim. Neft. Mashinostr.* **2005**, *6*, 10.
[205] A. S. Puschnov, *Chem. Pet. Eng.* **2006**, *42*, 14.
[206] N.-S. Cheng, *Powder Technol.* **2011**, *210*, 261.
[207] L. Meng, Y. Jiao, S. Li, *Powder Technol.* **2016**, *292*, 176.
[208] S. Torquato, T. M. Truskett, P. G. Debenedetti, *Phys. Rev. Lett.* **2000**, *84*, 2064.
[209] G. Y. Onoda, E. G. Liniger, *Phys. Rev. Lett.* **1990**, *64*, 2727.
[210] W. D. Treadwell, *Chem. Zentralbl.* **1913**, *1*, 857.
[211] H. Susskind, W. Becker, *Nature* **1966**, *212*, 1564.
[212] J. D. Bernal, J. L. Finney, *Nature* **1967**, *214*, 265.
[213] H. Zhao, X. An, Q. Qian, Y. Wu, L. Wang, W. Li, X. Yang, *Part. Sci. Technol.* **2019**, *37*, 251.
[214] Z. Xie, X. An, Y. Wu, L. Wang, Q. Qian, X. Yang, *Powder Technol.* **2017**, *317*, 13.
[215] C. X. Li, X. Z. An, R. Y. Yang, R. P. Zou, A. B. Yu, *Powder Technol.* **2011**, *208*, 617.
[216] Q. Qian, X. An, Y. Wang, Y. Wu, L. Wang, *Particuology* **2016**, *29*, 120.
[217] S. Debbas, H. Rumpf, *Chem. Eng. Sci.* **1966**, *21*, 583.
[218] S. Sharma, M. D. Mantle, L. F. Gladden, J. M. Winterbottom, *Chem. Eng. Sci.* **2001**, *56*, 587.
[219] G. Lumay, N. Vandewalle, *Phys. Rev. E* **2004**, *70*, 051314.
[220] J. Baker, A. Kudrolli, *Phys. Rev. E* **2010**, *82*, 061304.
[221] E. Ben-Naim, J. B. Knight, E. R. Nowak, H. M. Jaeger, S. R. Nagel, *Phys. D* **1998**, *123*, 380.
[222] E. Caglioti, V. Loreto, H. J. Herrmann, M. Nicodemi, *Phys. Rev. Lett.* **1997**, *79*, 1575.
[223] M. Bazmi, S. H. Hashemabadi, M. Bayat, *Transp. Porous Media* **2013**, *97*, 119.
[224] E. Harris, *Patent GB 606867*, **1946**.
[225] J. C. Macrae, W. A. Gray, *Br. J. Appl. Phys.* **1961**, *12*, 164.
[226] W. Zhang, K. E. Thompson, A. H. Reed, L. Beenken, *Chem. Eng. Sci.* **2006**, *61*, 8060.
[227] G. G. Brown, *Unit Operations*, 1st ed., Wiley, New York **1950**.
[228] A. B. Yu, N. Standish, *Powder Technol.* **1993**, *74*, 205.
[229] P.-Y. Lanfrey, Z. V. Kuzeljevic, M. P. Dudukovic, *Chem. Eng. Sci.* **2010**, *65*, 1891.
[230] N. Chikhi, R. Clavier, J.-P. Laurent, F. Fichot, M. Quintard, *Ann. Nucl. Energy* **2016**, *94*, 422.
[231] R. P. Zou, A. B. Yu, *Powder Technol.* **1996**, *88*, 71.
[232] M. Gan, N. Gopinathan, X. Jia, R. A. Williams, *KONA Powder Part. J.* **2004**, *22*, 82.
[233] F. M. Schaller, M. Neudecker, M. Saadatfar, G. Delaney, K. Mecke, G. E. Schröder-Turk, M. Schröter, *Am. Inst. Phys. Conf. Proc.* **2013**, *1542*, 377.

[234] T. Ikegami, *J. Am. Ceram. Soc.* **1996**, *79*, 148.
[235] A. G. Athanassiadis, M. Z. Miskin, P. Kaplan, N. Rodenberg, S. H. Lee, J. Merritt, E. Brown, J. Amend, H. Lipson, H. M. Jaeger, *Soft Matter* **2014**, *10*, 48.
[236] T. Allen, *Particle Size Measurement*. Powder Technology, 1st ed., Springer, Dordrecht, The Netherlands **1990**.
[237] H. Wadell, *J. Geol.* **1935**, *43*, 250.
[238] A. B. Yu, R. P. Zou, N. Standish, *J. Am. Ceram. Soc.* **1992**, *75*, 2765.
[239] R. Aoki, M. Suzuki, *Powder Technol.* **1971**, *4*, 102.
[240] J. V. Milewski, *PhD thesis*, Rutgers University, Rutgers, NJ **1973**.
[241] R. P. Zou, A. B. Yu, *Chem. Eng. Sci.* **1996**, *51*, 1177.
[242] J. Warren, R. M. German, P. U. Gummerson, D. A. Gustafson Eds., *Modern Development in Powder Metallurgy*, Vol. 18, Metal Powder Industries Federation, Princeton, NJ **1988**.
[243] J. G. Parkhouse, A. Kelly, *Proc. R. Soc. A* **1995**, *451*, 737.
[244] J. Blouwolff, S. Fraden, *Europhys. Lett.* **2006**, *76*, 1095.
[245] O. Rahli, L. Tadrist, R. Blanc, *C. R. Acad. Sci. Ser. IIb: Mec. Phys. Astron.* **1999**, *327*, 725.
[246] M. Novellani, R. Santini, L. Tadrist, *Eur. Phys. J. B* **2000**, *13*, 571.
[247] K. E. Evans, A. G. Gibson, *Compos. Sci. Technol.* **1986**, *25*, 149.
[248] H. Tangri, Y. Guo, J. S. Curtis, *Powder Technol.* **2017**, *317*, 72.
[249] M. Nardin, E. Papirer, J. Schultz, *Powder Technol.* **1985**, *44*, 131.
[250] R. Billet, M. Schultes, *Chem. Eng. Res. Des.* **1999**, *77*, 498.
[251] D. J. Gunn, *Chem. Eng. Sci.* **1987**, *42*, 363.
[252] J. Bear, *Dynamic of Fluids in Porous Media*, 1st ed., Elsevier, New York **1972**.
[253] O. Umnova, K. Attenborough, K. M. Li, *J. Acoust. Soc. Am.* **2000**, *107*, 3113.
[254] M. J. Yun, B. M. Yu, B. Zhang, M. T. Huang, *Chin. Phys. Lett.* **2005**, *22*, 1464.
[255] M. Matyka, A. Khalili, Z. Koza, *Phys. Rev. E* **2008**, *78*, 026306.
[256] W. Sobieski, S. Lipinski, *Tech. Sci.* **2017**, *20*, 75.
[257] M. Matyka, Z. Koza, *AIP Conf. Proc.* **2012**, *1453*, 17.
[258] H. Heywood, *Symposium on Particle Size Analysis, Supplement*, Vol. 25, Institution of Chemical Engineers, London, UK **1947**, p. 14.
[259] W. H. M. Robins, *Br. J. Appl. Phys.* **1954**, *5*, S82.
[260] J. K. Beddow, M. Kostelnik, H. H. Hausner, *Advances in Powder Metallurgy*, Vol. 4, Plenum Press, New York **1971**.
[261] C.-R. Chang, J. K. Beddow, M.-J. Yin, A. F. Vetter, G. Butters, D. L. O. Smith, *Particle Characterization in Technology*, 2nd ed., CRC Press, Boca Raton, FL **1984**.
[262] F. Benyahia, *Part. Sci. Technol.* **1996**, *14*, 221.
[263] J. Comiti, M. Renaud, *Chem. Eng. Sci.* **1989**, *44*, 1539.
[264] C. Xia, K. Zhu, Y. Cao, H. Sun, B. Kou, Y. Wang, *Soft Matter* **2014**, *10*, 990.
[265] Z. Wang, A. Afacan, K. Nandakumar, K. T. Chuang, *Chem. Eng. Process.* **2001**, *40*, 209.
[266] W. Man, A. Donev, F. H. Stillinger, M. T. Sullivan, W. B. Russel, D. Heeger, S. Inati, S. Torquato, P. M. Chaikin, *Phys. Rev. Lett.* **2005**, *94*, 198001.
[267] A. Jaoshvili, A. Esakia, M. Porrati, P. M. Chaikin, *Phys. Rev. Lett.* **2010**, *104*, 185501.
[268] G. D. Wehinger, S. T. Kolaczkowski, L. Schmalhorst, D. Beton, L. Torkuhl, *Chem. Eng. J.* **2019**, *373*, 709.
[269] E. A. Foumeny, F. Benyahia, *Heat Recovery Syst. CHP* **1991**, *11*, 127.
[270] C. W. Crawford, O. A. Plumb, *J. Fluids Eng.* **1986**, *108*, 343.
[271] A. Donev, I. Cisse, D. Sachs, E. A. Variano, F. H. Stillinger, R. Connelly, S. Torquato, P. M. Chaikin, *Science* **2004**, *303*, 990.
[272] M. Niu, T. Akiyama, R. Takahashi, J. Yagi, *AIChE J.* **1996**, *42*, 1181.
[273] N. Zobel, T. Eppinger, F. Behrendt, M. Kraume, *Chem. Eng. Sci.* **2012**, *71*, 212.
[274] J. D. McWhirter, M. E. Crawford, D. E. Kleins, *Transp. Porous Media* **1997**, *27*, 99.
[275] W. M. Visscher, M. Bolsterli, *Nature* **1972**, *239*, 504.
[276] G. T. Nolan, P. E. Kavanagh, *Powder Technol.* **1992**, *72*, 149.
[277] A. Yang, C. T. Miller, L. D. Turcoliver, *Phys. Rev. E* **1996**, *53*, 1516.
[278] H. P. Zhu, Z. Y. Zhou, R. Y. Yang, A. B. Yu, *Chem. Eng. Sci.* **2008**, *63*, 5728.
[279] P. A. Cundall, O. D. L. Strack, *Geotechnique* **1979**, *29*, 47.
[280] G. Lu, J. R. Third, C. R. Müller, *Chem. Eng. Sci.* **2015**, *127*, 425.
[281] S. Zhao, X. Zhou, W. Liu, C. Lai, *Particuology* **2015**, *23*, 109.
[282] M. Kodam, R. Bharadwaj, J. Curtis, B. Hancock, C. Wassgren, *Chem. Eng. Sci.* **2010**, *65*, 5852.
[283] M. Kodam, R. Bharadwaj, J. Curtis, B. Hancock, C. Wassgren, *Chem. Eng. Sci.* **2010**, *65*, 5863.
[284] Y. Guo, C. Wassgren, W. Ketterhagen, B. Hancock, J. Curtis, *Powder Technol.* **2012**, *228*, 193.
[285] J. Zhao, S. Li, P. Lu, L. Meng, T. Li, H. Zhu, *Powder Technol.* **2011**, *214*, 500.
[286] Y. Wu, X. An, A. B. Yu, *Powder Technol.* **2017**, *314*, 89.
[287] G. D. Wehinger, C. Fütterer, M. Kraume, *Ind. Eng. Chem. Res.* **2017**, *56*, 87.
[288] M. V. Tabib, S. T. Johansen, S. Amini, *Ind. Eng. Chem. Res.* **2013**, *52*, 12041.
[289] S. Li, J. Zhao, P. Lu, Y. Xie, *Chin. Sci. Bull.* **2010**, *55*, 114.
[290] X. Garcia, L. T. Akanji, M. J. Blunt, S. K. Matthai, J. P. Latham, *Phys. Rev. E* **2009**, *80*, 021304.
[291] R. Caulkin, W. Tian, M. Pasha, A. Hassanpour, X. Jia, *Comput. Chem. Eng.* **2015**, *76*, 160.
[292] R. A. Williams, X. Jia, *Part. Sci. Technol.* **2003**, *21*, 195.
[293] X. Jia, M. Gan, R. A. Williams, D. Rhodes, *Powder Technol.* **2007**, *174*, 10.
[294] X. Jia, R. A. Williams, *Powder Technol.* **2001**, *120*, 175.
[295] A. C. J. Korte, H. J. H. Brouwers, *Powder Technol.* **2013**, *233*, 319.
[296] B. Partopour, A. G. Dixon, *Powder Technol.* **2017**, *322*, 258.
[297] G. Boccardo, F. Augier, Y. Haroun, D. Ferré, D. Marchisio, *Chem. Eng. J.* **2015**, *279*, 809.
[298] J. Fernengel, J. Seckendorff, O. Hinrichsen, *Proceedings of the 28th European Symp. on Computer Aided Process Engineering* **2018**, *43*, 97.
[299] S. Flaischlen, G. D. Wehinger, *ChemEngineering* **2019**, *3*, 52.
[300] T. Eppinger, K. Seidler, M. Kraume, *Chem. Eng. J.* **2011**, *166*, 324.
[301] L. W. Rong, K. J. Dong, A. B. Yu, *Chem. Eng. Sci.* **2013**, *99*, 44.
[302] R. K. Reddy, J. B. Joshi, *Particuology* **2010**, *8*, 37.
[303] A. Pavlišič, R. Ceglar, A. Pohar, B. Likozar, *Powder Technol.* **2018**, *328*, 130.

[304] R. Mohanty, S. Mohanty, B. K. Mishra, *J. Taiwan Inst. Chem. Eng.* **2016**, *63*, 71.
[305] M. Marek, *Chem. Eng. Sci.* **2017**, *161*, 382.
[306] P. Magnico, *Chem. Eng. Sci.* **2003**, *58*, 5005.
[307] S. Khirevich, A. Höltzel, D. Hlushkou, U. Tallarek, *Anal. Chem.* **2007**, *79*, 9340.
[308] L. He, D. K. Tafti, K. Nagendra, *Powder Technol.* **2017**, *313*, 332.
[309] H. Freund, T. Zeiser, F. Huber, E. Klemm, G. Brenner, F. Durst, G. Emig, *Chem. Eng. Sci.* **2003**, *58*, 903.
[310] S. Das, N. G. Deen, J. A. M. Kuipers, *Chem. Eng. J.* **2018**, *334*, 741.
[311] D. Coelho, J.-F. Thovert, P. M. Adler, *Phys. Rev. E* **1997**, *55*, 1959.
[312] M. Zhang, H. Dong, Z. Geng, *Chem. Eng. Res. Des.* **2018**, *132*, 149.
[313] M. T. Zambon, D. A. Asensio, G. F. Barreta, G. D. Mazza, *Ind. Eng. Chem. Res.* **2014**, *53*, 19052.
[314] M. Behnam, A. G. Dixon, M. Nijemeisland, E. H. Stitt, *Ind. Eng. Chem. Res.* **2013**, *52*, 15244.
[315] M. E. Taskin, A. G. Dixon, E. H. Stitt, *Numer. Heat Transfer Part A* **2007**, *52*, 203.
[316] A. Singhal, S. Cloete, S. Radl, R. Quinta-Ferreira, S. Amini, *Chem. Eng. Sci.* **2017**, *172*, 1.
[317] S. J. P. Romkes, F. M. Dautzenberg, C. M. Bleek, H. P. A. Calis, *Chem. Eng. J.* **2003**, *96*, 3.
[318] S. A. Logtenberg, M. Nijemeisland, A. G. Dixon, *Chem. Eng. Sci.* **1999**, *54*, 2433.
[319] Y. Dong, B. Sosna, O. Korup, F. Rosowski, R. Horn, *Chem. Eng. J.* **2017**, *317*, 204.
[320] A. G. Dixon, G. Walls, H. Stanness, M. Nijemeisland, E. H. Stitt, *Chem. Eng. J.* **2012**, *200-202*, 344.
[321] G. D. Wehinger, T. Eppinger, M. Kraume, *Chem. Eng. Sci.* **2015**, *122*, 197.
[322] G. D. Wehinger, T. Eppinger, M. Kraume, *Chem. Ing. Tech.* **2015**, *87*, 734.
[323] M. Behnam, A. G. Dixon, P. M. Wright, M. Nijemeisland, E. H. Stitt, *Chem. Eng. J.* **2012**, *207–208*, 690.
[324] A. G. Dixon, M. E. Taskin, M. Nijemeisland, E. H. Stitt, *Ind. Eng. Chem. Res.* **2010**, *49*, 9012.
[325] A. G. Dixon, *Chem. Eng. Res. Des.* **2014**, *92*, 1279.
[326] B. Partopour, A. G. Dixon, *Comput. Chem. Eng.* **2016**, *88*, 126.
[327] A. H. Mahmoudi, F. Hoffmann, B. Peters, X. Besseron, *Int. Commun. Heat Mass Transfer* **2016**, *71*, 20.
[328] G. M. Karthik, V. V. Buwa, *AIChE J.* **2017**, *63*, 366.
[329] A. G. Dixon, J. Boudreau, A. Rocheleau, A. Troupel, M. E. Taskin, M. Nijemeisland, E. H. Stitt, *Ind. Eng. Chem. Res.* **2012**, *51*, 15839.
[330] K. M. Brunner, H. D. Perez, R. P. S. Peguin, J. C. Duncan, L. D. Harrison, C. H. Bartholomew, W. C. Hecker, *Ind. Eng. Chem. Res.* **2015**, *54*, 2902.
[331] F. Augier, F. Idoux, J. Y. Delenne, *Chem. Eng. Sci.* **2010**, *65*, 1055.
[332] G. E. Mueller, *Powder Technol.* **2005**, *159*, 105.
[333] G. W. Delaney, P. W. Cleary, *Europhys. Lett.* **2010**, *89*, 34002.
[334] Z.-Y. Zhou, R.-P. Zou, D. Pinson, A.-B. Yu, *Ind. Eng. Chem. Res.* **2011**, *50*, 9787.
[335] W. Nan, Y. Wang, Y. Liu, H. Tang, *Adv. Powder Technol.* **2015**, *26*, 527.
[336] E. M. Moghaddam, E. A. Foumeny, A. I. Stankiewicz, J. T. Padding, *Ind. Eng. Chem. Res.* **2018**, *57*, 14988.
[337] R. Guises, J. Xiang, J.-P. Latham, A. Munjiza, *Granular Matter* **2009**, *11*, 281.
[338] Z. Yan, S. K. Wilkinson, E. H. Stitt, M. Marigo, *Comput. Part. Mech.* **2015**, *2*, 283.
[339] M. Marigo, E. H. Stitt, *KONA Powder Part. J.* **2015**, *32*, 236.
[340] Q. Qian, L. Wang, X. An, Y. Wu, J. Wang, H. Zhao, X. Yang, *Powder Technol.* **2018**, *325*, 151.
[341] P. Philippe, D. Bideau, *Phys. Rev. E* **2001**, *63*, 051304.
[342] L. Pournin, M. Weber, M. Tsukahara, J.-A. Ferrez, M. Ramaioli, T. M. Liebling, *Granular Matter* **2005**, *7*, 119.
[343] D. Gou, X. An, X. Yang, H. Fu, H. Zhang, *Powder Technol.* **2017**, *322*, 177.
[344] Z. Xie, X. An, X. Yang, C. Li, Y. Shen, *Powder Technol.* **2019**, *344*, 514.
[345] J. Zhao, S. Li, R. Zou, A. Yu, *Soft Matter* **2012**, *8*, 1003.
[346] A. Wouterse, S. Luding, A. P. Philipse, *Granular Matter* **2009**, *11*, 169.
[347] A. Wouterse, S. R. Williams, A. P. Philipse, *J. Phys.: Condens. Matter* **2007**, *19*, 406215.
[348] S. R. Williams, A. P. Philipse, *Phys. Rev. E* **2003**, *67*, 051301.
[349] J. D. Sherwood, *J. Phys. A: Math. Gen.* **1997**, *30*, L839.
[350] W. I. Salvat, N. J. Mariani, G. F. Barreto, O. M. Martínez, *Catal. Today* **2005**, *107–108*, 513.
[351] P. L. Spedding, R. M. Spencer, *Comput. Chem. Eng.* **1995**, *19*, 43.
[352] K. Schnitzlein, *Chem. Eng. Sci.* **2001**, *56*, 579.
[353] S. C. Reyes, E. Iglesia, *Chem. Eng. Sci.* **1991**, *46*, 1089.
[354] G. E. Mueller, *Powder Technol.* **1997**, *92*, 179.
[355] B. Gong, Y. Feng, H. Liao, Y. Liu, X. Wang, K. Feng, *Fusion Eng. Des.* **2017**, *121*, 256.
[356] Q. Qian, X. An, H. Zhao, K. Dong, X. Yang, *Powder Technol.* **2019**, *343*, 79.
[357] S. Zhao, N. Zhang, X. Zhou, L. Zhang, *Powder Technol.* **2017**, *310*, 175.
[358] J. Zhao, S. Li, W. Jin, X. Zhou, *Phys. Rev. E* **2012**, *86*, 031307.
[359] J. Lathan, Y. Lu, A. Munjiza, *Geotechnique* **2001**, *51*, 871.
[360] S. Li, J. Zhao, X. Zhou, *Chin. Phys. Lett.* **2008**, *25*, 1724.
[361] P. Niegodajew, M. Marek, *Powder Technol.* **2016**, *297*, 193.
[362] W. Nan, Y. Wang, Y. Ge, J. Wang, *Powder Technol.* **2014**, *261*, 210.
[363] S. C. McGrother, D. C. Williamson, G. Jackson, *J. Chem. Phys.* **1996**, *104*, 6755.
[364] L. Liu, Z. Li, Y. Jiao, S. Li, *Soft Matter* **2017**, *13*, 748.
[365] A. V. Kyrylyuk, A. P. Philipse, *Phys. Status Solidi A* **2011**, *208*, 2299.
[366] Y. Jiao, S. Torquato, *Phys. Rev. E* **2011**, *84*, 041309.
[367] Y. Jiao, F. H. Stillinger, S. Torquato, *Phys. Rev. E* **2010**, *81*, 041304.
[368] J. Q. Gan, A. B. You, Z. Y. Zhou, *Chem. Eng. Sci.* **2016**, *156*, 64.
[369] K. E. Evans, M. D. Ferrar, *J. Phys. D: Appl. Phys.* **1989**, *22*, 354.
[370] K. Dong, C. Wang, A. Yu, *Chem. Eng. Sci.* **2015**, *126*, 500.
[371] K. Desmond, S. V. Franklin, *Phys. Rev. E* **2006**, *73*, 031306.
[372] C. Ferreiro-Córdova, J. S. Duijneveldt, *J. Chem. Eng. Data* **2014**, *59*, 3055.
[373] P. M. Chaikin, A. Donev, W. Man, F. H. Stillinger, S. Torquato, *Ind. Eng. Chem. Res.* **2006**, *45*, 6960.

[374] P. Bolhuis, D. Frenkel, *J. Chem. Phys.* **1997**, *106*, 666.
[375] R. Blaak, D. Frenkel, B. M. Mulder, *J. Chem. Phys.* **1999**, *110*, 11652.
[376] A. Baule, R. Mari, L. Bo, L. Portal, H. A. Makse, *Nat. Commun.* **2013**, *4*, 2194.
[377] M. Bargiel, *Computational Science - ICCS 2008* (Eds: M. Bubak, G. D. van Albada, J. Dongarra, P. M. A. Sloot), Springer, Berlin, Heidelberg **2008**, p. 126.
[378] A. V. Kyrylyuk, M. A. Haar, L. Rossi, A. Wouterse, A. P. Philipse, *Soft Matter* **2011**, *7*, 1671.
[379] C. R. A. Abreu, F. W. Tavares, M. Castier, *Powder Technol.* **2003**, *134*, 167.
[380] J. O. Freeman, S. Peterson, C. Cao, Y. Wang, S. V. Franklin, E. R. Weeks, *Granular Matter* **2019**, *21*, 84.
[381] Y. Kallus, *Soft Matter* **2016**, *12*, 4123.
[382] J. Q. Gan, Z. Y. Zhou, A. B. Yu, *Powder Technol.* **2017**, *320*, 610.
[383] X. L. Deng, R. N. Davé, *Granular Matter* **2013**, *15*, 401.
[384] F. Dorai, C. M. Teixeira, M. Rolland, E. Climent, M. Marcoux, A. Wachs, *Chem. Eng. Sci.* **2015**, *129*, 180.

How to cite this article: von Seckendorff J, Hinrichsen O. Review on the structure of random packed-beds. *Can J Chem Eng*. 2021;1–31. https://doi.org/10.1002/cjce.23959